Spring 2020

Impedance Analysis of Tissues in nsPEF Treatment for Cancer Therapy

Edwin Ayobami Oshin
Old Dominion University, eoshi001@odu.edu

IMPEDANCE ANALYSIS OF TISSUES IN NSPEF TREATMENT FOR CANCER THERAPY

by

Edwin Ayobami Oshin
B.ENG. October 2018, Afe Babalola University, Nigeria

A Thesis Submitted to the Faculty of
Old Dominion University in Partial Fulfillment of the
Requirements for the Degree of

MASTER OF SCIENCE

BIOMEDICAL ENGINEERING

OLD DOMINION UNIVERSITY
May 2020

Approved by:

Chunqi Jiang (Director)

Siqi Guo (Member)

Bulysheva Anna (Member)

Barbara Hargrave (Member)

ABSTRACT

IMPEDANCE ANALYSIS OF TISSUES IN NSPEF TREATMENT FOR CANCER THERAPY

Edwin Ayobami Oshin
Old Dominion University, 2020
Director: Dr. Chunqi Jiang

Nanosecond pulsed electric field (nsPEF) for cancer therapy is characterized by applications of high voltage pulses with low pulsed energy to induce non-thermal effects on tissues such as tumor ablation. It nonthermally treats tissues via electroporation. Electroporation is the increase in permeabilization of a cell membrane due to the application of high pulsed electric field. The objective of this study was to investigate the effect of nsPEF on tissue by monitoring the tissue's impedance in real-time. Potato slices (both untreated and electroporated), and tumors extracted from female BALBc mice were studied. 100ns, 1-10kV pulses were applied to the tissues using a four-pin electrode at a pulse repetition frequency of 3Hz. The impedance change during the treatment was recorded by a custom made V-I monitor, and a network analyzer measured the impedance before and after treatment over a frequency range of 100kHz to 30MHz. In addition, system calibration was conducted to ensure the accuracy of the measurements. This includes determination of the attenuation offered by the V-I monitor measured to be 60dB and the cell constant K which represents the geometry of the four-pin electrode measured to be $0.8453 cm^{-1}$ (±0.02cm). Results show that the impedance of tissue reduced with increasing number of pulses and voltage applied, up to 44.4% and 22.3% decrease in the impedance of potato and tumor tissues were respectively observed. Also, the impedance values were higher at lower frequencies compared to those at higher frequencies. This is due to the high resistance of the membrane at low frequencies.

This thesis is dedicated to my brother, sisters, and parent for the support they gave me during my graduate study. Without them, I wouldn't be where I am today. They are the driving force behind the success I may have achieved here at Old Dominion University. Also, thanks to Vivian for being a great source of encouragement when I felt down. I am forever indebted to these people.

ACKNOWLEDGMENTS

This thesis would never have been possible without the support and guidance of people that helped me in completion of my Master's degree. A big thank-you goes to my supervisor, Dr. Chunqi Jiang, for accepting me into her lab and always encouraging me. She has been a strong support towards the completion of my masters. I would like to thank Dr. Siqi Guo, my co-advisor, for willing to allow me to work with him. He gave tremendous support towards my thesis. A big thank-you to my other committee members Dr. Barbara Hargrave and Dr. Bulysheva Anna who have been always ready to help me. They contributed a lot to the completion of my Master's study. Also, I would like to appreciate my friends and colleagues, James Hornef, David Alderman, Shutong Song, and Ankit Baingane for their encouragement, support, and assistance.

TABLE OF CONTENTS

Page

LIST OF TABLES

LIST OF FIGURES

Figure Page

CHAPTER 1

INTRODUCTION

1.1 ORGANIZATION & CONTRIBUTION

This thesis explores the effect of nanosecond pulsed electric field (nsPEF) in the treatment of biological tissues by assessing the impedance changes with respect to the number of pulses and the applied electric field. Potato tissues were treated with 100ns, 1-80 pulses with electric field 1-5kV at a frequency of 3Hz. The breast tumors were treated with 100ns, 1000-1200 pulses with electric field of 10kV, frequency 3Hz. The external field induces a transmembrane voltage, charging up the membrane like a capacitor, which is thought to induce pores. The formation of the pores is known as electroporation, which can be either reversible or irreversible. Impedance analysis of the treated samples can be used to monitor the degree of electroporation induced.

This thesis is organized as follows. First, an introduction to the subject of concern was done. This includes a comprehensive review of prior research works, a review of the history and progress achieved so far in the field, and a description of the grey areas yet to be explored. Secondly, the methodology for the study was discussed in detail. It explains the experimental setup, system characterization, sample collection, and data collection. After the experimental setup and methodology, the results of the experiment were presented. The system was carefully characterized to make sure results were accurate. Voltage and current waveforms and the impedance (real and imaginary) were measured and used to explain the effects of nsPEF on the samples. The effects were assessed for different applied electric potential, pulse number, and duration of pulses. Finally, the conclusions of the research were presented.

1.2 BACKGROUND

Pulsed electric field (PEF) processing is a growing technological method in the area of electromagnetics that shows at a lot of promise, especially for medical, environmental, and food applications [1,2]. The treatment is based on the application of an electric voltage across a biological material placed between two electrodes, forming an electric field that is dependent on the amount of electric voltage applied, the shape of the electrodes and the gap between electrodes [3]. PEF can be categorized into conventional PEF processing and nanosecond (nsPEF) processing. In the conventional PEF, the applied electric field charges up the cell membrane and causes pores to form temporarily, breaching the integrity of the membrane and allowing for foreign molecules that would not be able to enter the cell in the absence of an applied electric field to enter the cell. They are relatively long in the range of microseconds to milliseconds and with a low electric field (about 1kV/cm). However, nsPEF can be orders of magnitude shorter in the nanoseconds range and with a higher electric field (about 10-100 kV/cm) [4]. nsPEF is an extension of the conventional PEF and has different effects on the cell. Conventional PEF has its pronounced effect on the plasma membrane while nsPEF affects intracellular structures and functions as the pulse duration is below the charging time of the plasma membrane [3]. Nevertheless, nsPEF has effects on the plasma membrane that are direct nonbiological effects as well as secondary biological effects. While biological effects can be easily measured, the direct electric field effects are harder to determine because they cannot be detected by fluorophores and molecular probes are too large [5]. The effects of nsPEF can be measured on the plasma membrane (integrity, potential), endoplasmic reticulum (calcium mobilization), mitochondria (respiration), and nucleus (fluorescence changes, DNA damage, gene expression). Also, studies with tumors and tissues show slowed tumor growth to tumor regression [6].

One of the major questions that remains an actively investigated area is the cell-specific effect of nsPEF. It is generally known that unlike conventional PEF, the nsPEF effects are not dependent on the cell size, and also adherent cells have a higher threshold for nsPEF effects than cultured cells. Both PEFs result in electroporation of the cell, increasing the mass transfer of molecules and ions [1].

CHAPTER 2

LITERATURE REVIEW AND THEORETICAL FRAMEWORK

2.1 ELECTROPORATION

Electroporation, also known as electropermeabilization is the application of short pulses of a high external electric field to cells and tissues which creates nanoscale defects in the cell membrane [7]. The external field induces a transmembrane voltage, charging up the membrane like a capacitor, which is thought to induce pores. Electroporation has been studied for decades and has been used in the laboratory and food industry, but not until recently has it been applied to the field of interventional oncology.

2.1.1 HISTORY

The history of electroporation can be traced back to the middle of the eighteenth century when Nollet, in 1754, reported the first systematic observation of the appearance of red spots on human and animal skin that was exposed to electric sparks [8]. After this, interest in the effects of electricity on the biological system increased, mainly focusing on how electric currents applied to the spinal cord and muscle nerve preparations induced twitching and contraction [9]. In the nineteenth century, the first description of the bacterial effect of IRE was reported, using high voltage discharges to purify water; however, the mechanism behind the process was not understood. In the twentieth century, reports were made for the application of electricity to medicine. Not until the early 1900s was the phenomenon of electroporation characterized as inducing increased permeabilization of the cell membrane and the thermal and nonthermal effects of electricity on cells understood. Lee RC et al. distinguished the injuries due to the effect of electrical burns from the nonthermal electrical injuries caused by lightning, which is now thought

to be caused by electroporation [10]. In addition, two major discoveries were made in the early twentieth century to further understand electroporation: 1) advances in the understanding of the membrane as a dielectric structure by estimating the thickness of the membrane and assessing the electrical properties of red blood cells and 2) knowledge that electricity can generate both thermal and nonthermal biological effects [11]. During the second half of the twentieth century, the principle of electroporation for permeabilizing the cell membrane was used primarily in studies related to nerves and food sterilization. For example, Frankenhaeuser and Wid'en [12] in 1956, and Stampfli and Willi [13] in 1957 reported that changes in nerves damaged by an electric field can be explained by electrical conductivity. Stampfli and Huxley described the reversible and irreversible effects of electroporation on a frog nerve membrane, assessing the effect of changing the electrical pulse characteristics and measuring the consequent changes in the resistance, treating the membrane as a capacitor [9].

Still, in the late 1900s, a lot of research was conducted on reversible electroporation as it became a major technology in the medical and biological fields. In 1982, Neumann and colleagues used pulsed electric fields to temporarily permeabilize the cell membrane, creating a pore that allows the entrance of foreign substances into the cell [14]. This was done to induce cell fusion known as electrofusion and to transfer DNA into the cell known as electrotransfer. Reversible electroporation has long been established as a laboratory application for electrofusion and electrotransfer. It is done by placing the cells or tissue between two electrodes. An example is the plastic cuvettes with two aluminum electrodes on either side used for applying an electric field to cell suspensions. The viral delivery of DNA can be avoided by using bacterial and eukaryotic cells for DNA electrotransfer. While progress was being made to better understand electroporation, the research on the bacterial effect of IRE done in 1898 progressed, and by the 1960s electrical pulses

were commercially installed for non-thermal inactivation of bacteria. Sale and Hamilton contributed to this by describing the nonthermal effect of electric pulses, the optimal pulse variables needed to achieve this effect, and the underlying physiology responsible for the changes and poration of the membrane [9].

In the following decade, many advances were made not only to better understand the mechanism of electroporation but also to improve its efficiency and application methods. An example of such advances was the use of the square wave electroporator that can give precise and controlled adjustment of the amplitude and duration to be applied, giving optimal pulse parameters [15]. Also, in this decade, a combinational effect of the electric field and chemotherapeutic drugs such as bleomycin was done to improve drug delivery; this is referred to as electrochemotherapy (ECT) [16,17]. This was also used with DNA, and it yielded a novel clinical application known as gene electrotransfer (GET) [18].

Most of the advances made were in the reversible application of electroporation as Irreversible electroporation was seen as an unwanted extreme because it caused cell death. In recent years, reports show that IRE has a lot of advantages; not only did it cause cell death through necrosis but also from apoptosis. It was in the late 1990s that it was first suggested that irreversible electroporation can be useful as an ablation technique [19]. Nonthermal irreversible electroporation (NTIRE) has immerged as a new medical procedure of electroporation technology for the ablation of solid tumors.

2.1.2 MECHANISM OF ELECTROPORATION

I. Molecular Dynamics

As a consequence of the exposure of the membrane to an electric field, pores are created, so there are many theoretical descriptions to explain the mechanism underlying the phenomenon, some of which assume a certain kind of deformation of the lipid [20], a breakdown of interfaces between the domains with different lipid compositions [21], or membrane protein denaturalization [22], but none of these fully captures the mechanism. Electroporation is broadly chosen as the best description of the formation of pores in the lipid bilayer. As a result of the exposure of the bilayer to the electric field, a transmembrane voltage (TMV) is induced consisting of two components: 1) resulting from the rearrangement of the lipid heads and the adjacent water molecule tails [23] and 2) resulting from the redistribution of charges and ions as they accumulate on both sides of the bilayer, charging it as a capacitor [24]. The first component occurs within picoseconds and pulses much shorter than 1 microsecond while the second component occurs for pulses far longer, only reaching its upper level within microseconds [25].

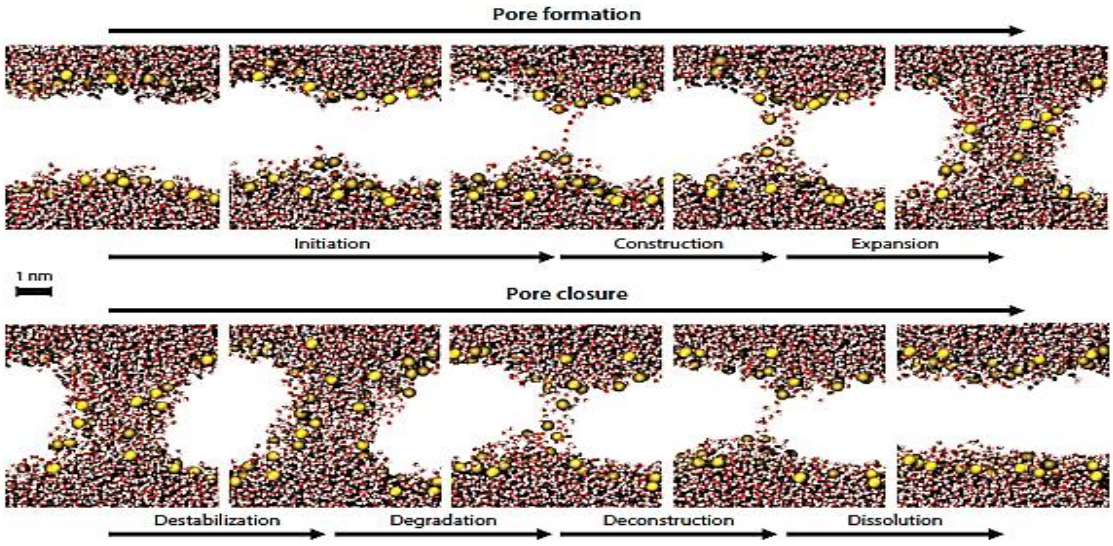

Figure 1: The Stages of Formation and Closure of Lipid Bilayer Electrically Induced Pore [6].

The pores that are formed in the bilayer as a result of the applied electric field are very small and have a radius of about several nanometers which is too small to be detected by optical microscopy; they are also metastable, making them too fragile to withstand the sample preparation required for electron microscopy of soft tissue, making it difficult to distinguish the pores from artifacts [26]. In contrast, molecular dynamics (MD) simulation is able to show evidence of the theory of pore formation (Figure 1). Over the last two decades, MD simulation has reached a level of both computing power and methodology proficiency to explain the mechanism of electroporation in silico. Therefore, MD simulations model the buildup of TMV induced by exposing a bilayer to an electric field depending on the pulse duration. For the first TMV component in the submicrosecond pulse duration, the TMV is generated by imposing an electric field E across the membrane which in practice will be imposing a force equal to the product of E

and the charge on every particle [27], while for the second component, lasting microseconds or milliseconds, the TMV is generated by imposing a net charge difference on both sides of the bilayer which in practice would be achieved by relocating several individual ions across the membrane [28]. The little setback of the MD simulation is that its capacity is too low to capture the billions of lipids in the membrane, so a smaller unit of hundreds to thousands is used with carefully defined ensemble conditions and boundary conditions [29].

II. Pore Formation and Resealing

As shown previously, electroporation entails the formation of pores in the cell membrane, assuming that they are formed randomly at different locations and different sizes due to the thermodynamics of the phospholipid molecules. The energy required to form a single pore of radius r is given by the classical surface physical chemistry, treating the lipid bilayer as an infinitely thin film without any internal structure [30]. This was derived from the work done by Deryagin and Gutop on soap film stability in the 1960s [30].

$$\Delta W_p(r) = 2\gamma\pi r - \pi r^2\Gamma \quad (1)$$

where the first term is the product of the pore perimeter $2\pi r$ and the line tension of the pore edge γ, which is the energy gained in the formation of the unit length of the pore boundary. This term is dependent on the internal membrane properties (elastic parameters), determined by the chemical structure of the membrane [31]. The second term is the product of the pore lumen area and the lateral tension Γ (energy per area of a flat pore-free membrane) exerted. Therefore, the pore formation energy for a single pore $\Delta W_p(r)$ is the difference between the energy gained in forming the outer edge of the pore and the energy reduction due to the cut of the circular patch from the membrane when the pore is formed. By definition, it is the activation energy barrier that must be

overcome to create a hydrophobic pore in the absence of a transmembrane voltage [11]. Cells do not self-rupture frequently because the activation energy barrier is very high, too high for the membrane to reach in the absence of an external field. When the radius exceeds a critical value (0.3 to 0.5nm), the activation barrier is exceeded and forms an aqueous pore which is how electroporation is initiated. Water molecules penetrate the lipid bilayer, and the adjacent lipids reorient their polar head group, pointing towards the water molecule, generating a stable hydrophilic pore. In addition, if the radius reaches a maximum critical level where $r^* = \frac{\gamma}{\Gamma}$, irreversible rupture of the membrane occurs known as irreversible electroporation (IRE) [32].

Pore formation is a stochastic process that occurs on a time scale of nano to microseconds and depends on a variety of parameters to determine the degree to which the electroporation is achieved. Some of the factors to consider are the duration of exposure to an external electric field, the size and orientation of the cell with respect to the electric field, the type of the cell exposed (cells with a wall such as plants and fungi will require extra induced voltage for poration), and the properties of the medium surrounding the cells [26]. Resealing of the pore is also a stochastic process but occurs over a much longer time compared to its formation. After the removal of the external electric field, the pores begin to close, and it is independent of the electric field. The pore closure is often completed within ten to hundreds of nanoseconds [33]. The resealing of the pores is only applicable to reversible electroporation and not irreversible electroporation which will be discussed in section 2.2

III. Transmembrane Voltage

The principle of electroporation is based on the induction of transmembrane potential (ITV) across a biological cell due to the application of PEF. For a regularly shaped cell (spherical),

with a radius r, exposed to a homogenous electric field E, the transmembrane potential difference as a function of time can be estimated by the equation

$$\mathrm{ITV} = \mathrm{f}.\,\mathrm{E_{ext}}.\,\mathrm{r}.\cos\theta(1 - \mathrm{e}^{-\mathrm{t}/\tau_\mathrm{m}}) \quad (2)$$

$$\tau_\mathrm{m} = \mathrm{r}.\,\mathrm{C_m}.\,(^{1}/_{2\sigma_\mathrm{e}} + {}^{1}/_{\sigma_\mathrm{i}}) \quad (3)$$

where f is a dimensionless form factor and τ_m is the charging time constant of the membrane, both of which can be expressed as a function of the electrical and geometrical properties of the cell [34] (under physiological conditions, $\mathrm{f} \approx 1.5$ and $\tau_\mathrm{m} \approx 0.5\ \mu\mathrm{s}$). $\mathrm{E_{ext}}$ is the external electric field strength as a function of time, θ is the polar angle with respect to the direction of the electric field, and t is the treatment time (Figure 2). The extracellular conductivity is critical to inducing an effect, and this influences the membrane charging time as shown in equation 3, where $\mathrm{C_m}$ is the membrane capacitance per unit area, σ_e is the external conductivity, and σ_i is the internal conductivity [35].

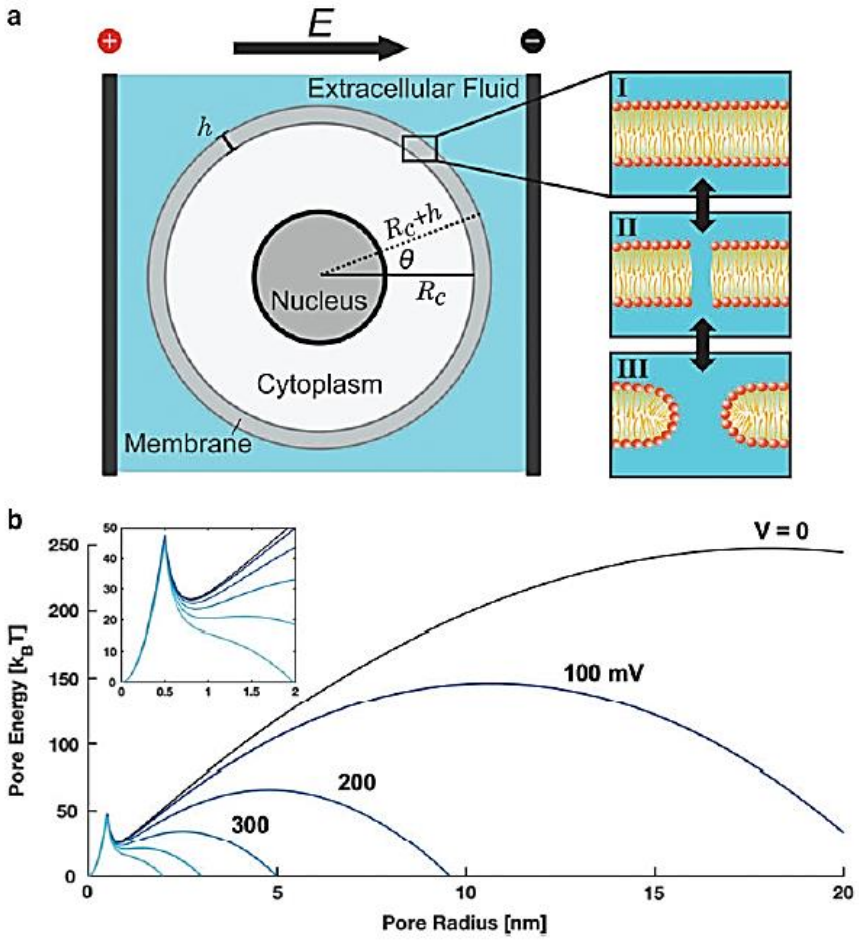

Figure 2: Factors Affecting the Behavior of the Cell Exposed to External Electric Field [36].

For non-spherical cells and cells close to each other, the ITV cannot be derived analytically. A more complex mathematical model will be required to estimate the pore size and determine whether the pore is reversible or irreversible. An easier alternative is to determine the ITV experimentally using a potentiometric dye [37].

2.2 RANGE OF EFFECTS CAUSED BY ELECTROPORATION

I. Reversible electroporation

The earliest reports of electroporation date as far back as over two centuries. In the reversible electroporation (RE), the electric field is applied to the cell membrane causing a transmembrane voltage to be induced, leading to the temporary formation of pores when the threshold is exceeded and forming molecular transport channels. After the external field is removed, the pore begins to close at a rate slower than the rate at which the pore was formed, ceasing the transport of molecules and leaving the cell viable. RE is used mainly in molecular biology, pores are created in the bilayer and specific molecules such as plasmids, dyes, drugs, proteins, antibodies, and nucleic acids are ingested into the cell [38]. This is the principle used in electrochemotherapy (ECT) and gene electrotransfer. In practice, relatively long pulses in the range of micro to milliseconds and low electric fields of about 1KV/cm or less are sufficient enough to produce the pores. Application of the external electric field can be done either by bringing the cells in contact with the electrodes delivering the field, or the cells can be placed in the field without contact with the electrode. In the latter, the ITV will only be a fraction of the voltage delivered by the electrode [26].

II. Irreversible Electroporation

Irreversible electroporation (IRE) involves the application of a very high electric field to the cells. When the applied ITV exceeds a certain threshold, nanopores are formed, causing an extensive transport of molecules, particularly intracellular content out of the cell through the pores. The resealing of the pores is so slow that the nanopores become permanent resulting in death due to the cell's inability to maintain homeostasis and eventual degradation of the cell [39]. Research involving IRE did not start until recently, but it has become one of the major areas of interest,

especially in medical research for tumor ablation. This has resulted in the development of commercially available IRE consoles used specifically for tissue ablation [40,41]. IRE can induce nonthermal cell death, and this is the primary motivation behind using it for tumor ablation. This idea of applying IRE for tumor ablation was first introduced about a decade ago in theoretical work done by Davalos RV et al., who used mathematical analysis to show that IRE can nonthermally ablate tissue without any thermal effect as compared to the traditional thermal methods [41].

Although these two ranges of electroporation (RE and IRE) partly overlap, they differ in their effects on cells. They depend on the duration of exposure and the applied field to cause a critical defect size in the membrane. The formation of a critical defect is dependent on the local mechanical stress, the membrane edge energy, the type of cell, the size, age and morphology, and the nature of the applied electric field (Figure 3). The nature of the electric field can vary by changing the frequency, amplitude, number of electrodes, number of pulses, and duration of the pulse [7].

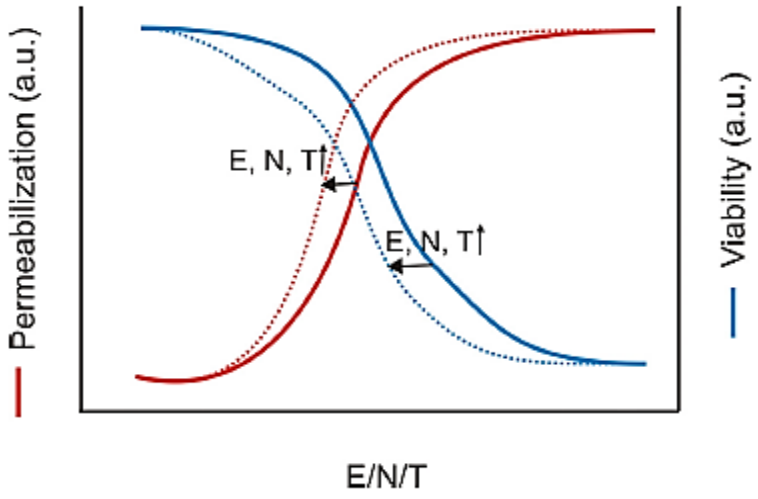

Figure 3: Graph Showing Cell Membrane Permeability and Viability [42].

2.3 APPLICATION OF ELECTROPORATION IN MEDICINE

I. Electrochemotherapy

Electrochemotherapy (ECT) has become a well-known treatment procedure in the medical field for local treatments in oncology [43]. Over 3000 patients, including both human and veterinary, have been treated with this application in the European Union [44]. Mir et al. in 1991 published the first work to demonstrate the safety, feasibility, and effectiveness of ECT [16]. This triggered many other groups in the U.S. to perform further studies [45, 46, 47]. ECT is based on the combinational effect of the aforementioned properties of reversible electroporation and chemotherapeutic agents. It uses electroporation for the delivery of non-permeant chemotherapeutic drugs into the cells, aiding their transmembrane transport leading to increased cytotoxicity of the cell. Basically, for ECT treatment to be administered to a patient, the patient first gets an intravenous or intratumoral administration of the anticancer drug. Some drugs

identified as most suitable for clinical testing are bleomycin by Mir et al. [18, 45] and cisplatin by Sersa et al. [48]. The drug is allowed to be evenly distributed over the vascular system and extracellular space of the tissue. Then electrodes are placed around or inside of the tissue to deliver electric pulses to the tissue, causing the creation of pores in the membrane, and thereby enabling the diffusion of the non-permeant anticancer drugs in the extracellular space into the cell. After removal of the external electric field, the membrane permeability will take a few seconds to minutes to return to its original state. The chemotherapeutic drugs in the intracellular space of the cell damage the cell, and bleomycin will cause multiple DNA breaks while cisplatin will cause intra and inter-strand DNA bonds [18, 49].

A lot of research has shown that there are several mechanisms that contribute to the overall efficiency of ECT besides the basic mechanism of increased membrane permeability. One is reduced blood flow, resulting in a vascular disruption effect of ECT [50]. Another effect is the release of tumor antigens which are exposed to the patient's immune system and trigger a tumor antigen directed immune response [51]. The effectiveness of this application has been shown in different tumor models, some resulting in complete regression and others in partial regression [52]. In 2013, an overall data analysis and systematic review of all the studies published through 2012 was done, and it was confirmed that ECT treatment has significantly higher effectiveness (about 50%) than just the chemotherapeutic injection. ECT resulted in the effectiveness of 84.1% objective response (this includes both complete and partial regression) and 59.4% complete response (indicates complete regression) after a single treatment [53]. Multiple treatments can increase the effectiveness of the application.

II. Gene Electrotransfer

Another application of electroporation in medicine is gene electrotransfer (GET) to cells and tissues for gene therapy and vaccination. It appears as a complex and multistep process which requires: (i) electropermeabilization of the plasma membrane, (ii) electrophoretic migration of the DNA towards the membrane, (iii) DNA/membrane interaction, (iv) DNA translocation across the membrane, (v) intracellular migration of DNA through dense cell cytoplasm and, finally, (vi) DNA passage through the nuclear envelope and (vii) gene expression [42, 54, 55]. GET has been mainly used for DNA vaccination against cancer, infections, arthritis, multiple sclerosis, inflammation, and in regenerative medicine to genetically modify cells [42, 56, 57]. A lot of research has been done on the skin by Titomirov et al. [58], the liver by Heller R et al. [59], muscles and tumor tissue by Rols MP et al. [60], and many other targets including the brain, arteries, prostate, and kidney [56, 57], though efficiency varies with the different tissues.

In cancer treatment, GET works by delivering immunomodulatory genes, such as IL-12, IL-2, IL-15, and GM-CSF to target tumor vasculature, including vasostatin, endostatin and vascular endothelial growth factors (VEGF) which reduce or stops the supply of blood to the tumor [61, 62]. The effectiveness and safety of this application was demonstrated first by Daud et al. [63] who showed that IL-12 GET on cutaneous melanoma in humans was efficient in inducing tumor necrosis. Secondly, Spanggaard I et al. [64] demonstrated that intratumoral GET of plasmid AMEP with cutaneous melanoma metastasis showed safety in transfection and effectiveness of the molecules.

III. Transdermal Drug Delivery

Transdermal drug delivery has the potential to introduce drugs that cannot be administered intravenously or orally and overcomes the disadvantages of the other methods. The skin is made

up of several layers: the stratum corneum, viable epidermis, dermis, and subcutaneous tissue (hypodermis). These layers, especially the stratum corneum (the outermost layer of the skin) limits transdermal delivery. The stratum corneum has resistance orders of magnitude higher than deeper tissues. Therefore, overcoming this barrier needs to be achieved, with one of the methods being electroporation [65]. Upon the application of a high electric field across the skin, pores are formed across the stratum corneum, thereby rapidly reducing resistance and enhancing the delivery of drugs. The electroporation also causes electrophoresis of the skin. This is the movement of charged particles under the influence of the applied electric field [65]. The direct current from the applied electric field provides an electrophoretic force for the delivery of molecules across the corneum. The parameters that control the degree of skin permeabilization and transportation of drugs are the amount of electric field applied, pulse duration, pulse shape, and the number of pulses [66]. Care must be taken in selecting these electric pulse parameters and the electrodes used in order to prevent skin damage and pain. Although transdermal drug delivery is very effective and safe, it must be emphasized that it has poor reproducibility in the delivery of drugs [26].

IV. Non-thermal Tissue Ablation

Non-thermal tissue ablation employs the mechanism of IRE cell death. It is a minimally invasive surgical procedure in which the external pulsed electric field is applied to the tissue to cause irreversible damage to the cells by causing irreversible pores in the membrane. It is important to state that the phrasing ‘non-thermal’ does not mean the complete absence of thermal effects; rather, the effect can be controlled and kept to a minimum, thereby limiting thermal damage to vital structures surrounding the target tissue. Joule heating is the rise in temperature that occurs as a result of the current flowing through a conductor and is a function of the strength and time of the applied electric field, so it is inevitable. However, the proper application of non-thermal IRE

(NTIRE) treatment can maintain a sufficiently low temperature and prevent thermal damage to the surrounding structure [67]. One of the unique properties of NTIRE is its ability to preserve tissue architecture while sparing the tissue scaffold, large blood vessels [68, 69].

Davalos et al. in 2005 used mathematical modeling to predict that NTIRE can nonthermally ablate a clinically relevant volume of tissue [41]. This was further proven by experiments done in cell cultures [70], small animal models [71], large animal models [72], and recently in humans [73]. It is important to note that the effect varies for the different models and the treated organs. Treatment of pancreatic and prostate cancer showed 100% success; in the liver, it varied between 50 to 98.1%, while no treated lung tumors have been successfully ablated [26]. The exact mechanism of cell death induced by NTIRE is not known. Numerous studies have been done to investigate the mechanism of cell death, some by examining the histological morphology and staining [44] and some by transmission and electron microscopy, but they do not sufficiently give accurate proof as to the exact mechanism [74]. A general conclusion made is that it is a combination of several mechanisms including cellular necrosis [44], long term secondary apoptosis [74, 75], and a number of possible tertiary effects such as immune activation [76]. In general, both in vivo and in vitro experiments have shown that the mechanism of cell death induced by IRE is independent of the thermal effect generated from the pulsing [41, 44, 77].

2.4 ELECTROPORATION DETECTION MECHANISMS

2.4.1 IMPEDANCE MEASUREMENT

The structural integrity of tissue can be determined by the tissue's electrical impedance. It has been widely used to access the tissue condition in vitro, in vivo, and ex vivo [78-80]. Some work has been done on normal prostate tissue and malignant prostate cancer by Halter et al. [81], on malignant breast tissue by Kerner et al. [82], and on yeast cells by Soley et al. [80]. The

impedance spectrum of tissue is measured over a range of frequency points within a specific frequency band, and it gives information about the characteristics and integrity of the tissue or cell. An electrode, either two-electrode or four-electrode method is used to inject constant sinusoidal current (I) into the object under test, inducing a potential (V). In the four-electrode method, an alternating current is injected through two electrodes, and the ac potential is induced across the other two electrodes. The impedance is estimated by dividing the induced voltage by the current.

Different tissues have different electrical properties determined by the distribution of ions around the membrane, the tissue structure, and composition. Impedance measurement is used to better understand the properties of tissues, giving information about the effect of the pulsed electric field in electroporation of the membrane. On application of the external electric field, electroporation causes an immediate decrease in tissue impedance which can be used to monitor the outcome. Electroporation leads to a dielectric breakdown in the membrane causing structural reorganization of cell membranes and intracellular molecules. In this approach, the current generated by the electrode in contact with the tissue provides direct information about the change in impedance before and after the electroporation [83]. It is possible to monitor the changes in near real-time. The electrical impedance of a volume of tissue is utilized to give information about the cell population and how electroporation affects the cell membrane resistivity. Measurement of both the real Z’ (resistance) and imaginary Z’’ (capacitive reactance) part of the electrical impedance can be used to investigate the efficacy and damage to the cell membrane. In addition, electrical impedance tomography (EIT), magnetic resonance electrical impedance tomography (MREIT), and current density imaging (CDI) work based on this principle [84].

2.5 LIMITATIONS OF EXISTING STUDIES

A lot of improvements have been made in understanding electroporation, but some things remain unknown:

1) There is limited knowledge about how to set specific parameters for specific tissues and tumors. Improvements are being made in simulation to aid IRE ablation planning, but no sufficient results exist yet [43].
2) The underlying mechanism remains a subject of debate. Results from research done ex vivo and on animals shows that IRE can cause a substantial increase in temperature in the targeted tissue, and this has raised a lot of questions as to whether the poration of the membrane is responsible for the effect of IRE or the temperature rise [41, 44, 45].
3) Little knowledge is known about how the decreasing pulse duration results in a decreased effect on the cell membrane structure and function and increased effect in the intracellular environment [6].
4) The exact cell parameters that determine the efficiency of electroporation and how these parameters can be exploited for tumor treatment is not known [11].
5) Research shows that the resealing of pores occurs in several stages with time constants ranging from microseconds to tens of seconds, but none of the existing theories, experiments, or even molecular dynamics simulation in its simplified version can cover timescales that extensively [26, 46].

CHAPTER 3

METHODOLOGY

3.1 EXPERIMENTAL SETUP

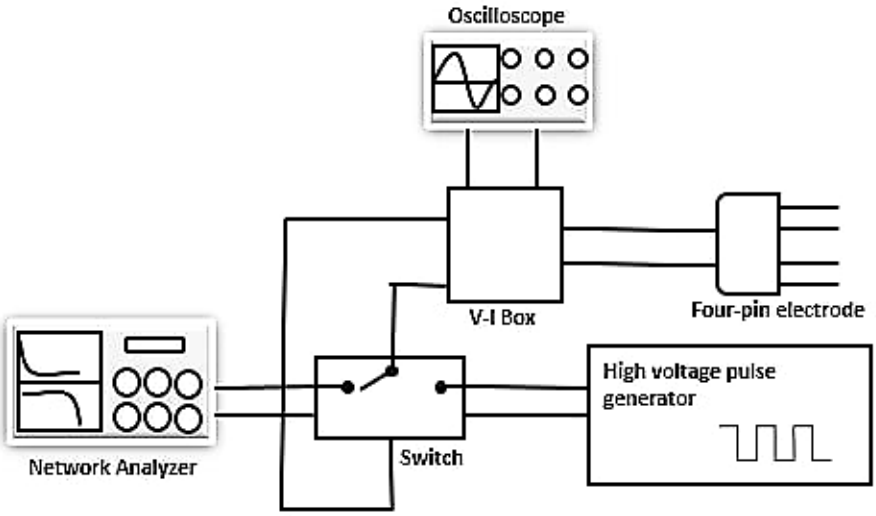

Figure 4: Schematic Presentation of the Experimental Setup.

For the ablation of samples, pulses were delivered to the sample using the four-needle electrode array of 7 x 5mm spacing. There is a 7mm gap between the anode and the cathode pins and 5mm between the two anode pins and two cathode pins. Potato slices having a thickness of 1.5cm were first examined. Potato tissue is a model commonly studied for electroporation because

on application of the electric field, the electroporated area becomes dark, making it easy to define the ablated area [85]. Then, breast tumors having a size of about 8-10mm in diameter and average volume of 250-300mm^3 were also examined for this study. Pulse parameters of duration 100ns, frequency 3Hz, pulse number 1000 and pulsed electric field between 1kV - 10kV were applied, depending on the experimental design (Figure 4).

3.2 MATERIALS AND INSTRUMENTS

Oscilloscope Model Waverunner 64Xi (LeCroy 600MHz), an E5071C Network analyzer (ENA series) model Agilent technologies, a laptop computer Lenovo ThinkPad core i7, a custom made switch, a voltage-current box, a Tektronix P6015A voltage probe, a four-needle electrode, and a custom made blumline 100ns pulsar were used.

3.3 ELECTRODE CONFIGURATION

A four-needle electrode arranged in an array of 7mm x 5mm spacing is used. The electrode was first drawn in inventor, the necessary dimensions for the needle holes, needle length adjustment, electrode height, and wiring system were carefully done. The inventor drawing helped save time when the machining was done in the machine shop. The electrode was made from four stainless steel needles of diameter 0.5mm held together by a solid teflon tube of diameter 25mm. Teflon was used to help prevent breakdown between the needles. In the standard configuration, the pins had an upright configuration. The needles were partially covered with polytetrafluoroethylene tubes to prevent surface flashover during the treatment and to prevent them from bending. The 5mm exposed area of the needle is the part inserted in the sample during measurement and treatment. Low resistive flexible copper wires (20AWG 150C 30KVDC) of equal length were used to connect the electrode to the system. A hollow teflon tube is attached to the electrode to allow for easy handling as shown in Figure 5.

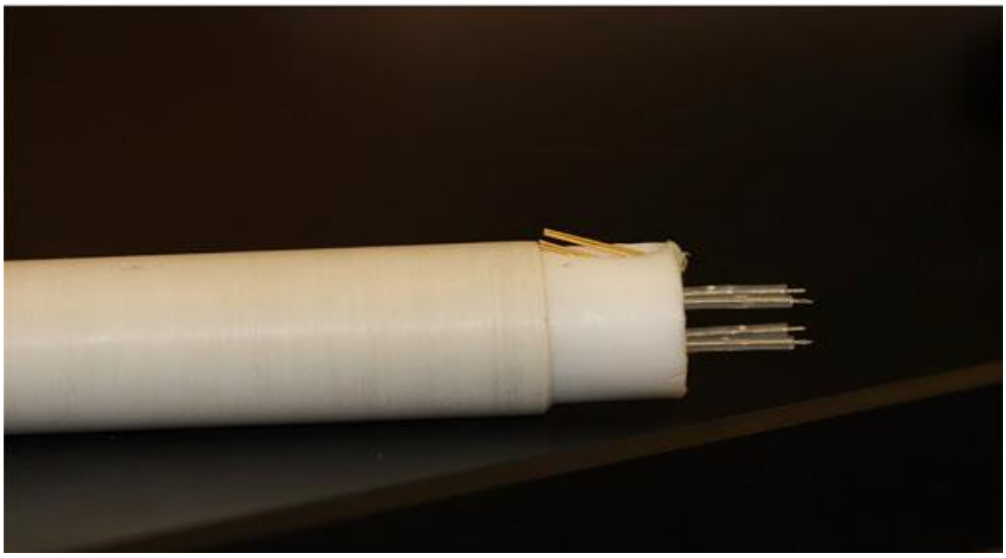

Figure 5: Four-Pin Electrode Used for Treatment.

3.4 MICE AND TUMOR MODEL

Female BALBc mice (6–8 weeks of age) were purchased from Jackson Laboratory. Mice were injected with 1×10^6 4T1-luc cells in 50µL Dulbecco's phosphate buffered saline (DPBS) on the left flank. The size of the primary tumor was assessed by digital calipers twice a week. Tumor volume was determined using the following formula: $V=\pi ab2/6$, where (a) is the longest diameter and (b) is the shortest diameter perpendicular to (a). Mice were euthanized at the end of the follow-up period, and the tumors were excised. All experimental protocols were approved by Old Dominion University Institutional Biosafety Committee (IBC) and Institutional Animal Care and Use Committee (IACUC). All experiments were performed in accordance with relevant guidelines and regulations.

3.5 IMPEDANCE AND CURRENT-VOLTAGE MEASUREMENT

The experimental setup for the impedance and current-voltage measurement is shown in Figure 4. High voltage square wave pulses were generated by a blumline pulsar. The impedance, amplitude |z| and phase angle φ before and after pulsing the sample were measured using a network analyzer (E5071C ENA Series, Agilent Technologies). Adequate calibration was done before taking any measurements to ensure the accuracy of the data. This is discussed in detail in section 3.9. For all the samples, the four-pin electrode connected to the network analyzer (NA) via a custom made switch was inserted in the tissue, and the impedance was measured. At room temperature, the samples (potato and breast tumor) were placed on a grounded platform, and the pins of the electrode were inserted into the sample. Only the exposed 5mm length of the pins was inserted, and care was taken to ensure the pins did not bend and were parallel to each other. The tissue electrical impedance was scanned over a frequency range of 100kHz to 30MHz, displayed as Real (resistive component) and Imaginary (capacitive reactance component). Without making changes to the system, the custom made switch is flipped to connect the electrode to the high voltage square wave pulser to apply the pulses to the tissues. 100ns, 1-5kV pulses were applied to the tissue at a pulse repetition frequency of 3Hz. The pulsed voltage and current were recorded during treatment using a customized V-I monitor connected to an oscilloscope (LeCroy waveRunner 64Xi, 600MHz 10GS/s).

To conduct phase two measurements, we needed to create a V-I monitor to monitor the voltage and current. The monitor was enclosed in a metal box, so the design of the monitor was focused on making sure none of the connectors were too close to the box because this would create arching and voltage breakdown. For easy manufacturing, one side of the box was chosen as input while the opposite side as the output where the four-needle electrode was connected. The other

two sides were drilled for the BNC female connectors to the oscilloscope. The V-I monitor consists of a resistive voltage divider circuit with a divider ratio of 1000:1 and a Pearson current probe with an output of 1volt per amp. A simple voltage divider circuit gives an output voltage that is a fraction of the input voltage. As shown in the circuit diagram below, a block containing two 50kΩ caddock resistors were connected in parallel to make a 25kΩ resistor, and the other block consisting of two 50Ω resistors were connected in parallel to make a 25Ω resistor. These two blocks were connected in series, and on the application of an input voltage, the output voltage was measured across the 25Ω resistor, shown in Figure 6. This works based on the principle of ohms law.

$$V_{out} = I * R = V_{in}\left(\frac{R_2}{R_1+R_2}\right) \quad (4)$$

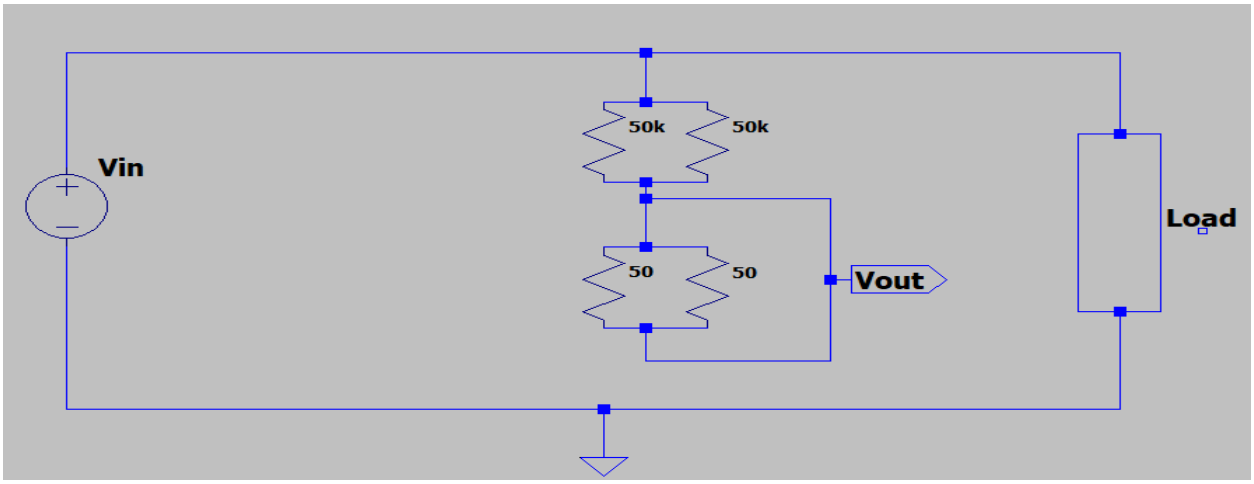

Figure 6: Circuit Diagram of V-I Monitor.

Both voltage and current were recorded with the digital oscilloscope using the autosave function to obtain a fast recording of the pulses. The ratio of the voltage and current provided information on the temporal change in impedance of the sample in real-time. After the treatment, the electrode was switched back to the NA for the third impedance measurement. The measurement was taken 3-6 seconds after the last pulse. Impedance was measured at a frequency range of 100kHz to 30MHz. In this study, the electrical impedance (Z) of russet potatoes and 4T1-luc breast tumors was conducted and the variations in Z(ω), tetha (ω), resistance R(ω), reactance X(ω), conductivity σ (ω), capacitance C(ω), and relative permittivity (ε_r), over the frequency range were studied.

3.6 SAMPLE COLLECTION AND PREPARATION

One of the materials studied was the Russet potato purchased from Walmart. They were stored at room temperature (20C) and relative air humidity (50-60%). Slices having a thickness of approximately 1.5cm were cut from the tubers of a potato and placed in a container of a water at room temperature, to keep all the samples under the same condition. Before treatment, each slice was taken out of the water and dampened using Kimwipes.

The other material studied is the breast cancer model. Female BALBc mice were purchased from Jackson Laboratory (Bar Harbor, ME, USA). The mice were injected with cell line 4T1-luc on the left flank to produce the tumors. The size of the tumor was monitored until it reached the criterion required. All experiments were conducted in accordance with relevant guidelines and regulations.

3.7 DATA COLLECTION

A custom made voltage-current monitor was inserted between the electrode and the high voltage pulse power supply for monitoring the voltage and the current supplied to the samples.

The V-I monitor was connected to a high-speed digital oscilloscope that autosaved the waveforms. The voltage and current waveforms were collected and imported into MATLAB where algorithms were written to process the data. The same applied to measurements done by the network analyzer; data was collected and processed using MATLAB. The algorithm determined the impedance change, permittivity, and conductivity after each treatment.

3.8 DIELECTRIC CONSTANT MEASUREMENT

All samples were analyzed using the network analyzer (E5071C ENA Series, Agilent Technologies) and the oscilloscope (LeCroy waveRunner 64Xi, 600MHz 10GS/s). The analyzer measured reactance X (ohms) and resistance R (Ohms) at frequencies between 0.1 to 30MHz. The experimental capacitance C and resistance R data were converted to relative permittivity $\varepsilon^{'}$ and conductivity $\sigma^{'}$ ($S.m^{-1}$) over the given frequency ω according to

$$\varepsilon'_{\omega} = \frac{C_{\omega} * K}{\varepsilon_0} \tag{5}$$

$$\sigma'_{\omega} = \frac{k}{R_{\omega}} \tag{6}$$

The conductivity σ'_{ω} reflects the properties of the tissue. The frequency dependent relationship between the impedance (z), conductivity ($\sigma^{'}_{\omega}$), and relative permittivity ($\varepsilon^{'}_{\omega}$) can be given by the expression

$$Z = Z' + j\omega Z'' = {}^{1}/_{(\sigma + j\omega\varepsilon_0\varepsilon_r)} \tag{7}$$

where Z, Z' and Z'' is the total impedance, real and imaginary component of Z respectively, ω is the radial frequency and ε_0 is the permittivity of free space ($8.854 \cdot 10^{-12}\ F \cdot m^{-1}$). K is the cell constant which reflects the geometry of the electrode. Different tissues have different electrical properties determined by the distribution of ions around the membrane. The conductivity is related

to the conduction current I_c developed due to the movement of ions in the intracellular space of the cell while the permittivity is related to the extent to which the bound charges I_d are polarized under the influence of the external electric field. These bound charges include the electrical ions on the membrane surface and polar molecules [86]. Tissue conductivity is calculated from the real parts of the tissue impedance measurement and the capacitance, and permittivity is calculated from the imaginary part.

3.9 SYSTEM CHARACTERIZATION

To ensure the accuracy of the measurements taken from the network analyzer and the V-I monitor, the characterization of the system is required. First, to characterize the NA, calibration had to be done at the needles of the electrode, as shown in Figure 7. A connector was made to connect the electrode to the open, short and load calibration kit of the NA. This will eliminate every additional impedance that the system (including the electrode system, the V-I monitor, and NA cable) might offer so that the impedance measurements taken will be that of just the sample.

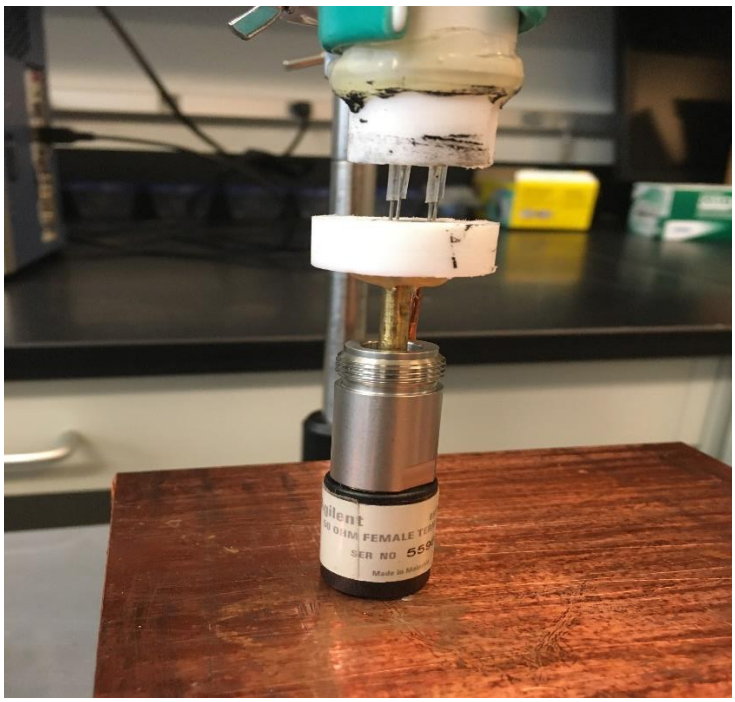

Figure 7: System Calibration at the Needles of the Electrode.

Secondly, to ensure the accuracy of the voltage-current measurement from the V-I monitor, the V-I monitor was connected directly to the NA, and the forward complex transmission coefficient S21 was measured to show the attenuation offered by the voltage divider circuit. Also, a standard Tektronix probe with the same expected attenuation was used alongside the V-I monitor to monitor the voltage to see if the waveforms match.

$$S21 = \frac{\text{Transmitted}}{\text{Incident}} \tag{8}$$

$$dB = 20\log\left(\frac{Vin}{Vout}\right) \tag{9}$$

Expected attenuation = 60dB

Thirdly, the cell constant K reflects the geometry of the electrode. It is assumed in theory that an electrode, at a given temperature, will have a specific K value, but in reality, the value may vary slightly. The variation may be due to the measured conductivity of the liquid, temperature, electrode polarization, occurrence of current paths spreading out of the electrode, the measuring frequency, and many other factors [87]. The recommended method for determining the value of K is based on the measurement of the resistance of a standard solution [88]. According to equation 11, the resistance (ohms) is divided by the standard known resistivity (ohms meter) to obtain K.

$$R = \rho \frac{L}{A} \tag{10}$$

$$K = \frac{R_{\omega}}{\rho_{\omega}} \tag{11}$$

To get constant K, sodium chloride (NaCl) solutions of different concentrations and known resistivity are used. The NaCl salt samples were measured using a high precision weighing balance. NaCl solutions with concentrations of 1%, 5%, 15%, 20%, were carefully prepared. These different concentrations were chosen because they have known standard resistivity values as obtained from the CRC Handbook of Chemistry and Physics, 91st edition. The concentration in mass percent was converted to Molar concentration using equation 12:

$$\text{Molar Conc (M)} = \%\text{g of NaCl} * \frac{1\text{mol NaCl}}{\text{weight of NaCl(g)}} * \frac{1}{\text{Vol of NaCl(L)}} \tag{12}$$

The weight of the NaCl salt used is 58.58g and a volume of 0.1L was made. Salt of 0.2g, 1g, 3g, 4g were carefully measured using the weighing balance and dissolved in distilled water to make 0.1L of NaCl solution. The different solutions were poured in a beaker and the rectangular (5 x 7mm) measuring cavity of the four needle electrode is placed in the solution. The measuring cavity

was 5mm deep in the solution as the needles were partially covered with polytetrafluoroethylene tubes. The impedance was measured using the network analyzer.

CHAPTER 4

RESULTS

4.1 SYSTEM CHARACTERIZATION

Calibration of the network analyzer was first performed to ensure the correctness of the measurements. Open, short and load calibration was done at the electrode needle and Figure 8 shows the measurements taken. Figure 8(a) represents the resistance and reactance after calibration of the system with no load at the electrode. It shows there is no reflection or impedance in the system. Figure 8(b) shows the resistance and reactance of the system with a 50ohm load at the electrode before calibration and after calibration. It is seen that before calibration, the measurement was inaccurate and varied over the different frequencies, but after calibration was done, it became constant, showing the exact resistance of 50ohms.

To ensure that the voltage divider circuit in the V-I monitor gave the appropriate output, the attenuation was measured using the NA. From equation 9, the expected attenuation is 60dB. This was confirmed from the S21 measurement done across the voltage divider circuit.

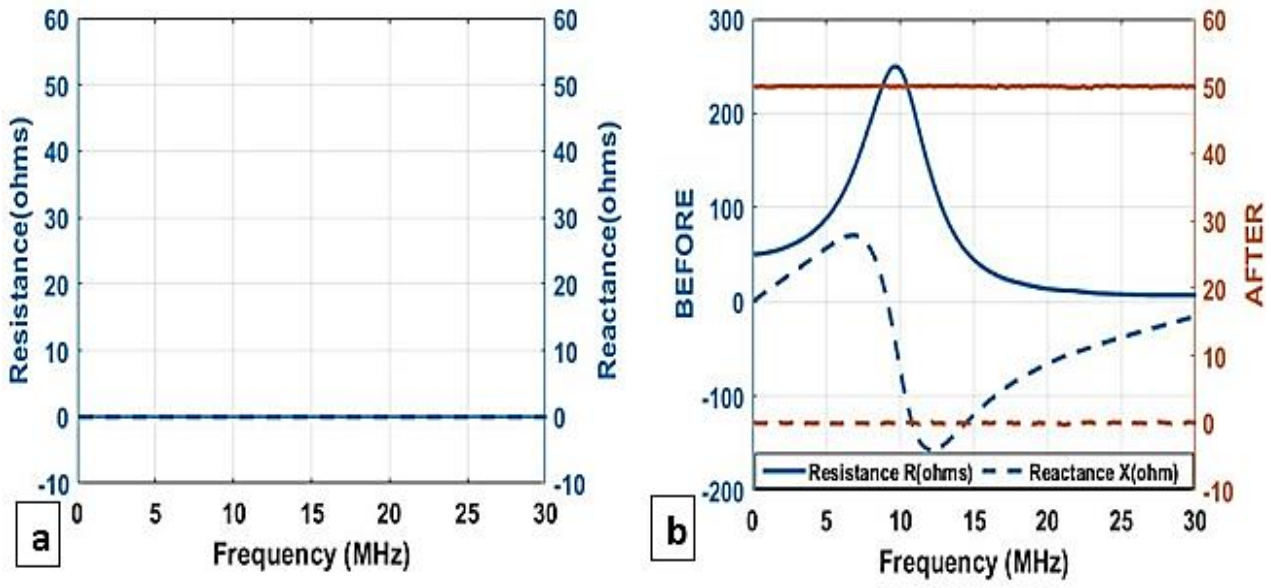

Figure 8: Characterization of the System Using a Network Analyzer.

As shown in Figure 9, the measured attenuation of 60dB matches our calculated value. Also, a voltage differential Tektronics probe is used together with the V-I monitor to measure the voltage applied to loads of different resistance (50ohm, 100ohm, and gel). The V-I monitor and the probe both gave similar waveforms shown in Figure 10.

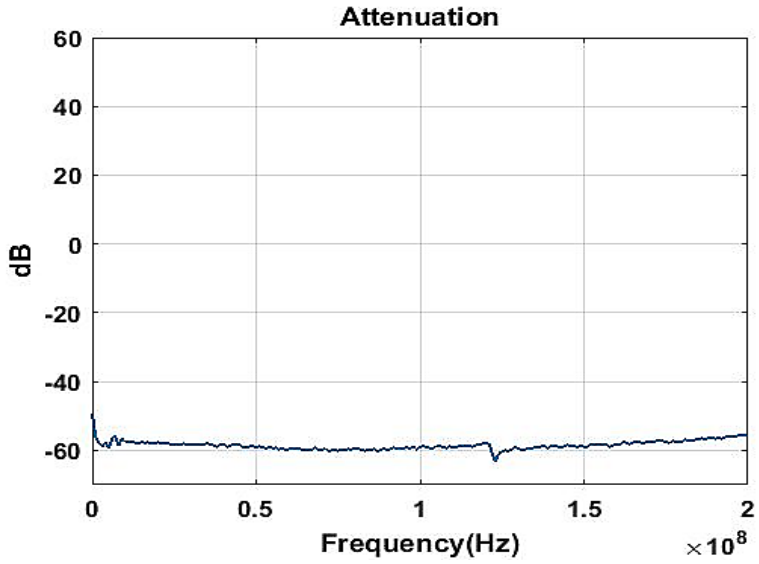

Figure 9: System Characterization of V-I Monitor.

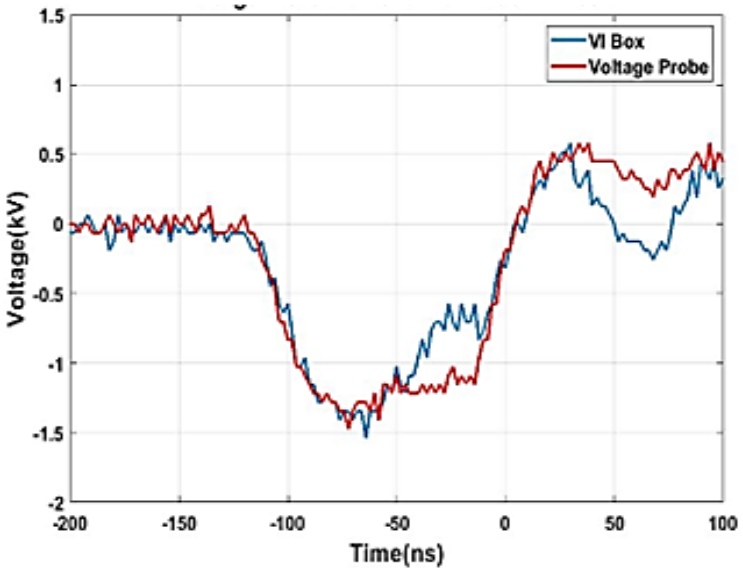

Figure 10: Graphs Showing Voltage Measurements Using V-I Monitor and Standard Probe.

To monitor the current applied to the samples, a Pearson current probe was used, with the high voltage line passing the core of the probe. The voltage and current measurements were used to calculate the resistance according to ohms law, and the resistance was calculated to be 52Ω for the 50Ω load and 103.5Ω for the 100Ω load.

The cell constant K reflects the geometry of the electrode. It depends on the current path which is affected by the geometry and volume of the sample. It has a unit of cm^{-1}. The impedance measurement is shown in Figure 11 below. The measurement shows that the resistance of the NaCl solution reduced with an increase in concentration. The more NaCl salt was added to the distilled water, the more electrolytes existed, which caused the solution to be more conductive. The resistance of each concentration is seen to be somewhat constant over the frequency range, proving that NaCl is purely resistive and is independent of signal frequency. Also, the reactance of the different concentrations of NaCl solution did not change significantly, showing that the solutions do not have a capacitive ability. The impedance at low frequency did not have a high steep, this is due to the absence of the dielectric barrier exhibited by the membrane of the tissue cells. The needles were cleaned after every measurement by rinsing with distilled water.

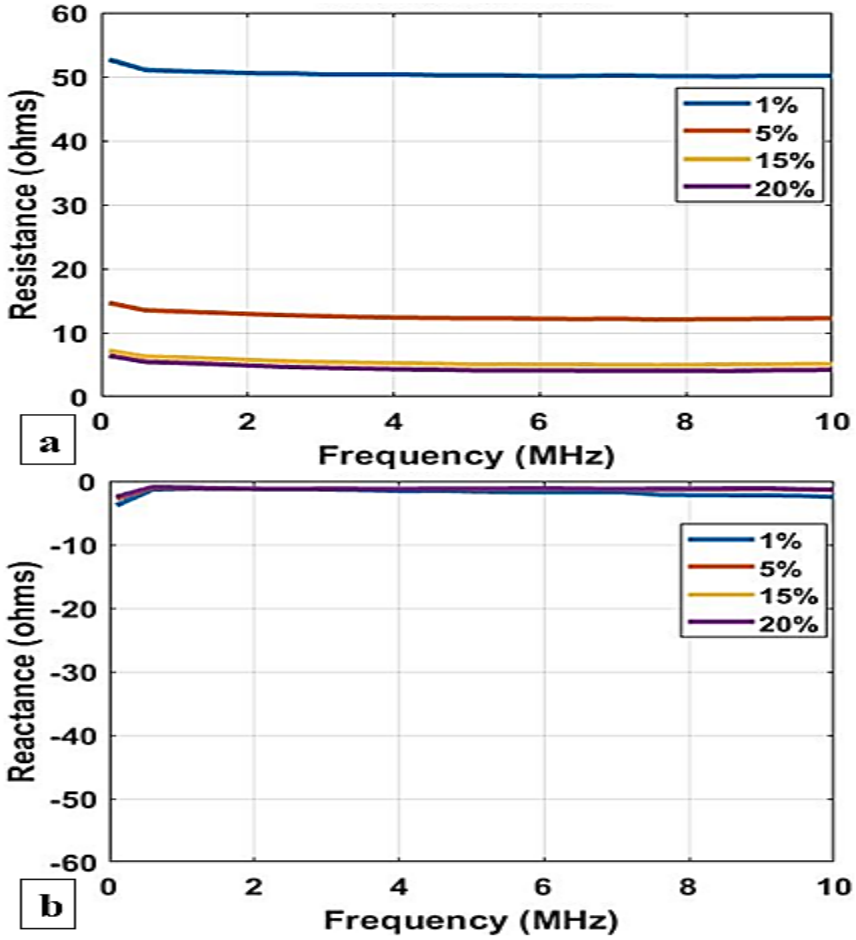

Figure 11: Impedance Measurements (Resistance R and Reactance X) of Different Concentrations of Sodium Chloride (NaCl) Solution.

Table 1: Electrical Resistivity of NaCl Aqueous Solutions.

Percentage Mass	**Molar Concentration (M)**	**Amount of NaCl salt (g)**	**Resistivity (Ω.cm)**	**Resistance (Ω)**	**Cell Constant K (cm^{-1})**
1%	0.1707	0.2	62.5	52.9	0.8464
5%	0.8535	1	14.27	12.2	0.85494
15%	2.5606	3	5.85	5	0.854701
20%	3.4141	4	4.9	4.1	0.836735

Measurements were carried out at room temperature (~ 20^0C). The resistance measured was divided by the known standard resistivity of the solutions to obtain the cell constant K of the electrode. The calculated values of K slightly varied by about ±0.02cm; therefore, an average value of K= 0.8453cm^{-1} was used in this study. Table 1 shows the measurements taken for the different concentrations.

4.2 TISSUE IMPEDANCE

Biological cells and tissues have a cell membrane that separates the intracellular from the extracellular environment. This makes the tissue structure exhibit two electrically conducting compartments – intracellular compartment and extracellular compartment. The conduction of electric current across the cell is inhibited by the membrane acting as a resistance to the flow. This opposition is frequency dependent; therefore, the impedance spectrum of the tissue is obtained over a frequency range of 100kHz to 30MHz, reflecting the properties of the tissue. When a high

pulsed electric field is applied across the membrane, the membrane is permeabilized as a result of the dielectric breakdown of the membrane.

The impedance variation Z of the potato tissue with an increasing number of pulse and applied voltage is shown in Figure 12 below at frequency range 100k – 30MHz. A zoomed in view at a frequency of 100k -1MHz is added to show the trend of impedance change with pulse number and voltage. A steep increase is observed at a lower frequency which is typical for tissues whose cells are interconnected [89]. The membrane of the cell is composed of an electrically non conducting lipid bilayer between two conducting protein layers, hence acting as an ultrathin capacitor surrounding the intracellular environment. On the application of the electric field, at low frequencies, the membrane is very resistive and low electric current will travel in the extracellular space surrounding the membrane [90]. At high frequencies, the resistance drops, and the impedance approaches zero, allowing the electric field to pass through the cell or tissue more uniformly. As the frequency increases, the membrane behaves as a capacitor, appearing as a short circuit.

$$Z = Z' + Z'' \tag{13}$$

$$Z'' = \frac{1}{2\pi fC} \tag{14}$$

When the resistance is high, the capacitive property is low, but when the resistance drops, the tissue becomes more capacitive. This property is observed in the potato tissue as seen in Figure 12. Up to 80 pulses were applied to the tissue. The tissue impedance was compared with that without pulses. The resistance is seen to reduce with the increasing number of pulses applied whereas the reactance increased.

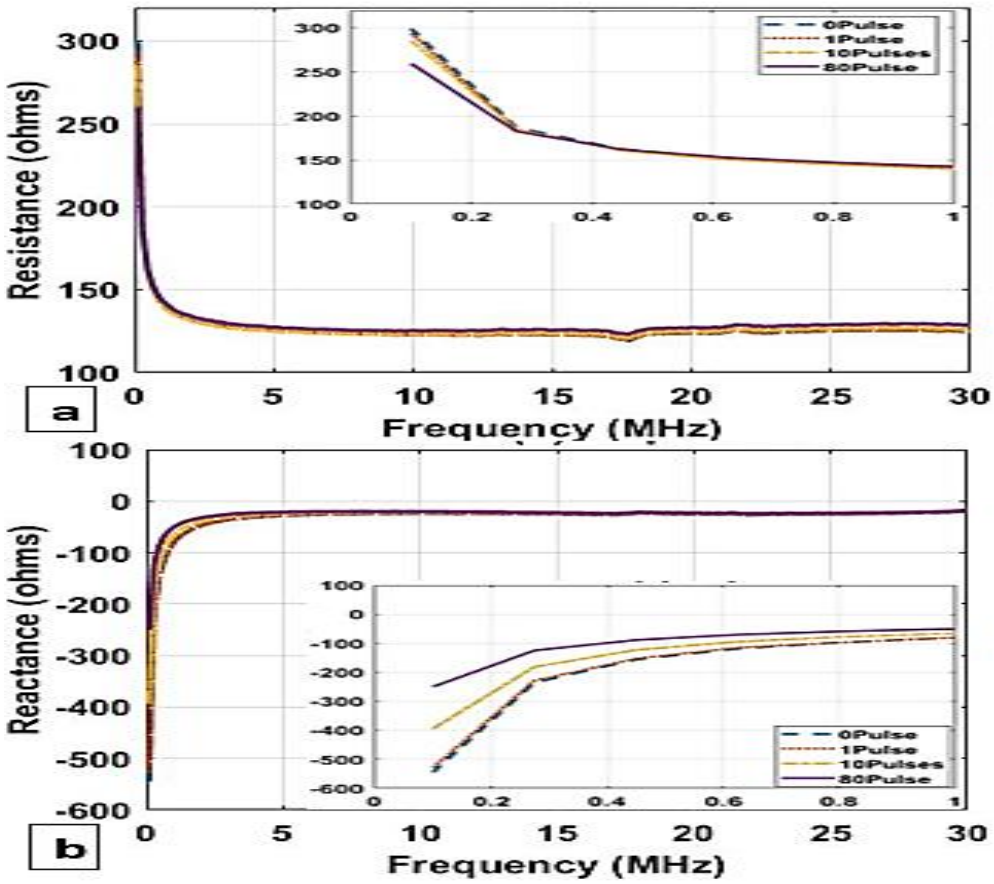

Figure 12: Impedance Measurement of Potato Tissue Over the Frequency Range at 1kV.

There was little to no difference between the impedance of tissues with a single pulse treatment and the no treatment group, signifying that a single pulse was not enough to cause substantial damage to the membrane. Also, different electric potentials were applied to the tissue – 1kV, 3kV, and 5kV – but only results for 1kV are shown here. With an increase in voltage, the resistance is seen to reduce (Figure 12a) and the reactance increases, approaching zero (Figure 12b). It is important to note that only results at frequency of 100kHz were used in this study due to the large scattering of data observed at lower frequencies [91].

The impedance measurements of the NA were compared to the voltage-current measurements of the oscilloscope. As shown in Figure 13b, the resistance calculated from the voltage-current waveform shows that the resistance drops with an increase in pulse number and applied voltage but after about 30pulses, no decrease is seen, signifying that the measurement using the voltage-current is not so accurate in monitoring the impedance of tissues.

The V-I monitor is not able to measure impedance effectively at a voltage too high. The inaccuracies from the calculated impedance in past experiments show that the V-I monitor performs best at lower voltages. The safe tested range is 300V to 1.5kV. The NA measurement, on the other hand, showed a decrease in impedance over the 80pulses (Figure 13a), and it is seen that the higher the voltage applied, the more the impedance drops. Also, the area ablated by the applied electric field at 4hours and 10hours before and after 80pulses is shown in Figure 13c. The control group with no pulses applied showed no ablation area. As shown for 1kV, the lesions are seen in the areas close to the insertion points of the electrodes. With 3kV, the lesion begins to extend to areas around the electrode and towards the center of the tissue. Also, at 5kV, more lesion is induced.

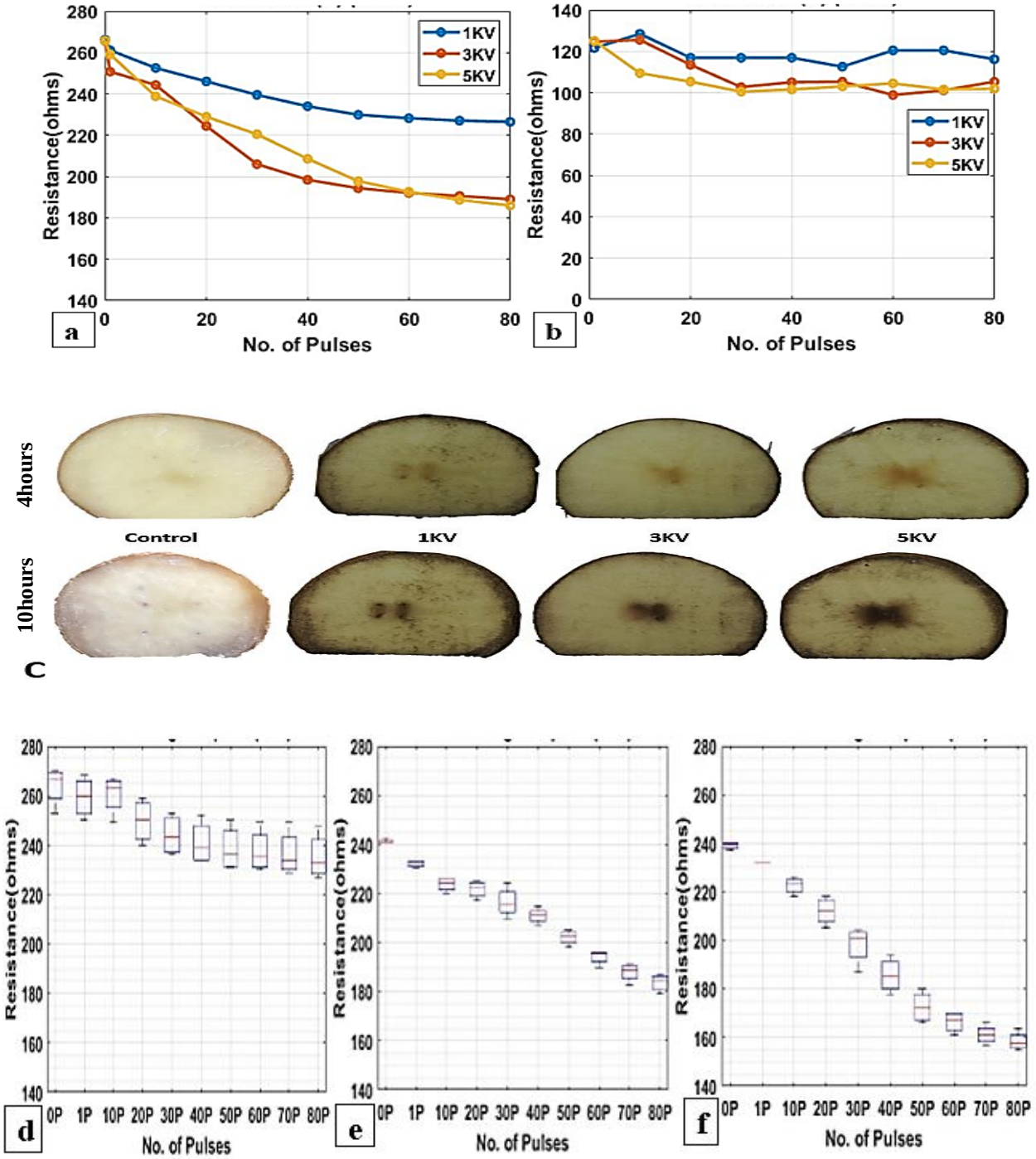

Figure 13: Impedance Trend and Ablation Area of Potato Tissue with Increasing Pulse Number and Electric Field.

No significant ablation was achieved with 1kV, and this correlates with the resistance measurement in Figure 13(a) which shows that there was only a little decrease in resistance after applying 1kV. Larger ablation size is seen with higher applied voltage. 10hours after treatment, the ablated area is more obvious due to more cell death overtime from the stress caused by the applied field. A minimum of seven repeats were done for each group, and Figure 13d, e, f, shows the variations in the results obtained from the NA. 1kV shows larger error bars compared to 3kV and 5kV (Figure 13d, e, f), further proving that no significant effect was caused to the tissue at 1kV. 1kV, 3kV, and 5Kv has a p value of 3.7405e-05, 1.1383e-21, and 2.4097e-22 respectively. The variations in the results obtained from the V-I monitor are shown in the appendix.

The correlation between the ablated area and the impedance drop is shown in Table 2. Resistance was measured immediately after application of 80 pulses. The length of the ablated area was measured parallel to the 5mm space between the two anode electrodes, and the width was measured parallel to the 7mm space between the anode and cathode electrodes. The area of the region ablated was also measured. These measurements were taken four hours and ten hours after treatment. The length, width, and area of the ablated region increased with an increase in applied voltage. Comparing the results taken at four hours and those at ten hours, the size at ten hours was about twice the size at four hours due to the stress caused by the applied voltage, causing more cells to die over time. Also, as the size of the ablated area increased, the resistance is seen to drop. The relationship between the resistance drop and the increase in ablated area was more of an exponential function than a linear one.

Table 2: Correlation of Ablated Area of Tissue with the Impedance Drop.

Groups	Resistance	4 Hours			10 Hours		
		Length	**Width**	**Area**	**Length**	**Width**	**Area**
Ctrl	266.1819	0	0	0	0	0	0
1kV	226.4592	3.2831	1.7501	4.3415	9.1816	10.5053	65.7433
3kV	188.9919	5.04725	2.2046	9.6210	9.4310	12.4363	84.6696
5kV	185.9558	7.858333	7.9850	32.9753	12.1223	15.8363	144.2730

The conductivity of all the samples was measured and compared to the conductivity after pulsing. The change in conductivity was obtained from the initial conductivity before pulsing σ_0 and conductivity after pulsing σ_N from equation 15.

$$\Delta\sigma_N = \frac{\sigma_N - \sigma_0}{\sigma_0} \quad (15)$$

Figure 14 shows the conductivity change $\Delta\sigma_N$ in the potato tissue at different applied electric potential and a different number of pulses. At the application of a single pulse, the change in conductivity is negligible; no significant change is observed over the different applied voltage. It is also observed that the conductivity did not change with increasing voltage, showing that little effect in electroporating the tissue was achieved with a single pulse. At 10 pulses, an increase in conductivity is seen, and the conductivity change increased with increasing applied voltage. A more significant change is seen with 80 pulses.

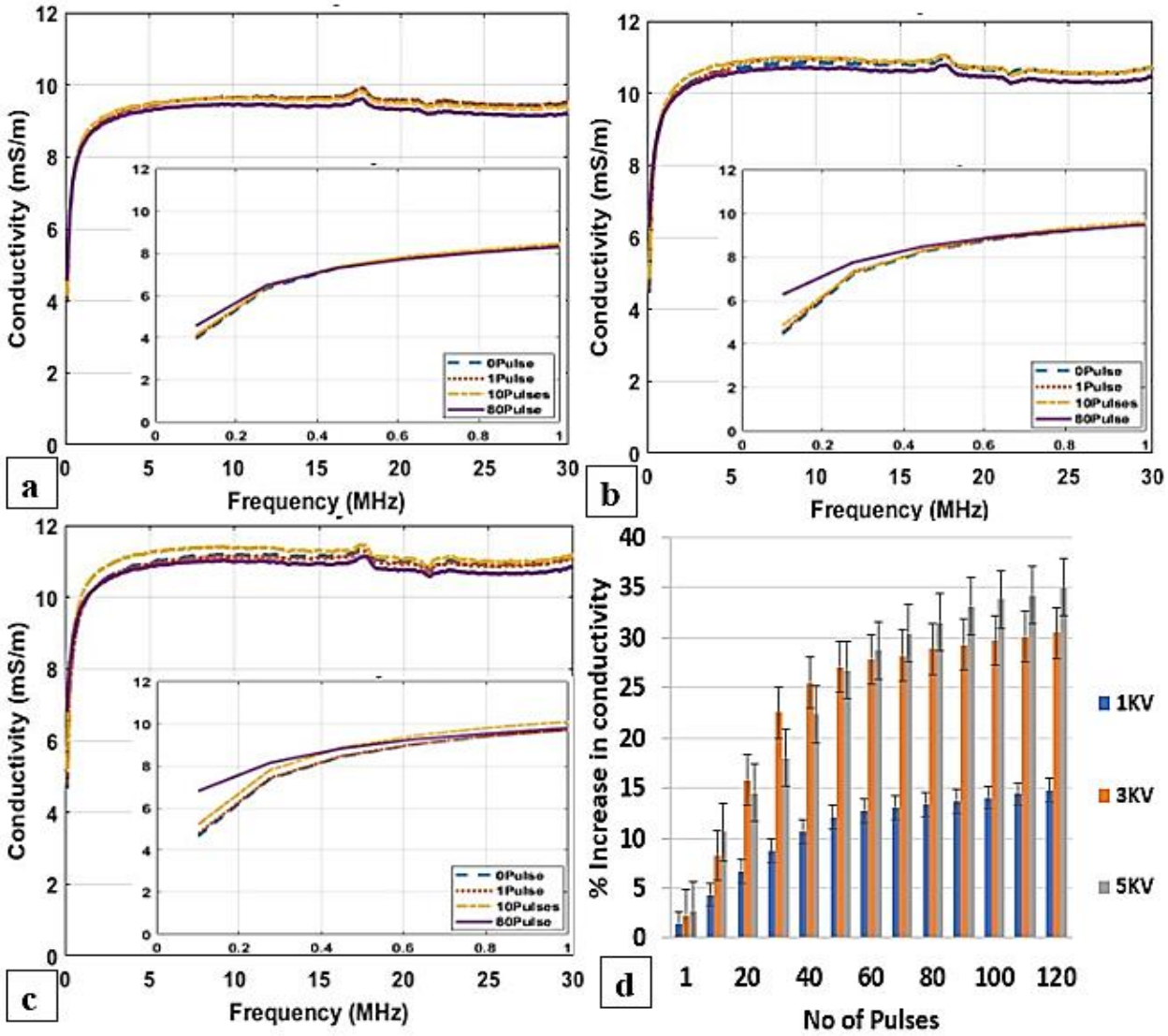

Figure 14: Conductivity of Potato Tissue After Application of Electric Field.

Treatments were done on breast tumors. 1000 to 1200, 100ns pulses 10KV were applied at a repetition frequency of 3Hz. A similar phenomenon as in the potato measurement was observed; a high steep in impedance is observed at lower frequencies, and as the frequency increased, the

impedance dropped drastically (Figure 15). Impedance measurement from the NA is shown in (a) and (b). Both cases of 1000pulses and 1200 pulses show a decrease in the resistance, but more decrease is seen with the higher number of pulses. Also, because the 1200pulses took a longer duration of application, the resistance is seen to drop more than for 1000pulses. As with the reactance, with a higher applied number of pulses, the reactance increased, making the tissue more capacitive.

According to the voltage and current measurement, the resistance is seen to decrease with an increasing number of pulses, supporting the impedance measurements done above. A percentage decrease of about 12.78% for 1000pulses and 22.3% for 1200pulses was obtained.

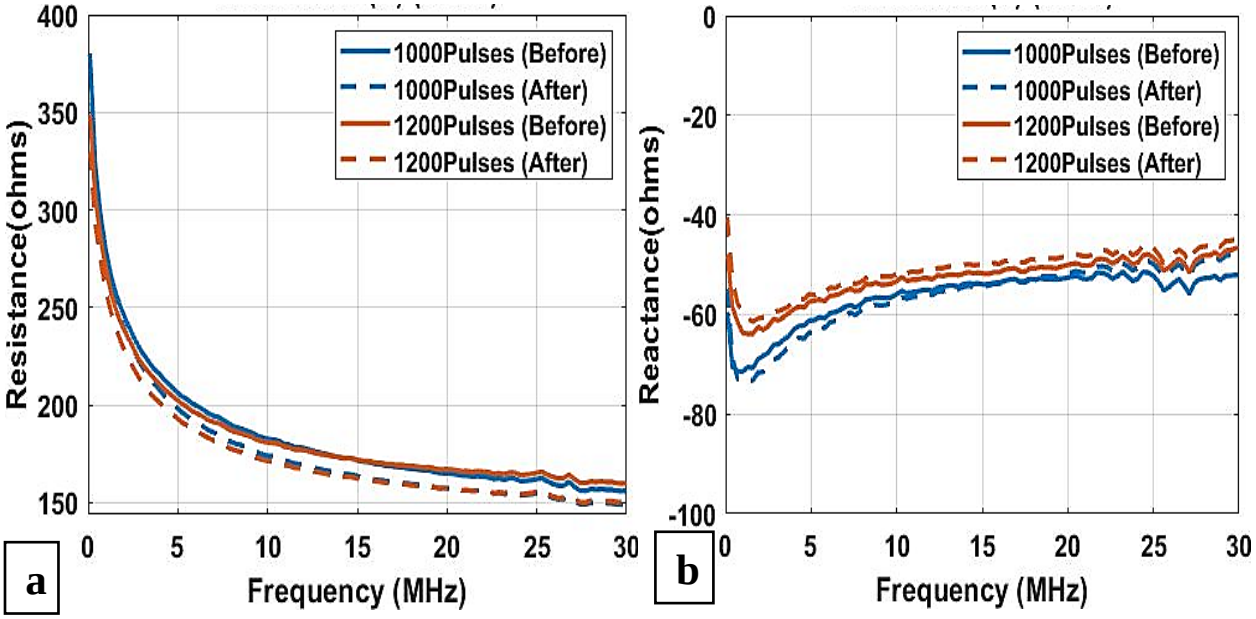

Figure 15: Impedance of Breast Tumor Before and After Application of 10kV 1000Pulses and 1200pulses.

CHAPTER 5

CONCLUSION

Electroporation is caused by the application of an external electric field to cells which induces a transmembrane voltage, charging the membrane like a capacitor. The transmembrane voltage induced results from the rearrangement of the lipid heads and the adjacent water molecule tails and the redistribution of the charges and ions on both sides of the bilayer. This causes the formation of pores which are formed randomly at different locations and different sizes due to the thermodynamics of the phospholipid molecules. When the radius exceeds a critical value (0.3 to 0.5nm), the activation barrier is exceeded and forms an aqueous pore which is how electroporation is initiated. At a maximum critical level of r, irreversible rupture of the membrane occurs known as irreversible electroporation. The resealing of the pores is so slow that the nanopores become permanent resulting in death due to the cell's inability to maintain homeostasis and eventual degradation of the cell. Some of the factors to consider are the duration of exposure to an external electric field, the size and orientation of the cell with respect to the electric field, the type of the cell exposed (cells with a wall such as plants and fungi will require extra induced voltage for poration), and the properties of the medium surrounding the cells. The nature of the electric field can vary by changing the frequency, amplitude, number of electrodes, number of pulses, and duration of the pulse.

The structural integrity of tissue can be determined by the tissue's electrical impedance. The impedance spectrum of tissue is measured over a range of frequency points within a specific frequency band, and it gives information about the characteristics and integrity of the tissue or cell. Measurement of both the real $Z^{'}$ (resistance) and imaginary $Z^{''}$ (capacitive reactance) part of the

electrical impedance can be used to investigate the efficacy and damage to the cell membrane. In this study, potato tissues and breast tumors were studied. The impedance was measured over frequencies between 0.1 to 30MHz. The experimental capacitance C and resistance R data were converted to relative permittivity $\varepsilon^{'}$ and conductivity $\sigma^{'}$ ($S.m^{-1}$) over the given frequency. The conductivity is related to the conduction current I_c developed due to the movement of ions in the intracellular space of the cell while the permittivity is related to the extent to which the bound charges I_d are polarized under the influence of the external electric field. However, before measurements were taken, the system was characterized to ensure the accuracy of the results.

Pulse parameters of duration 100ns, frequency 3Hz, pulse number 1000 and pulsed electric field between 1kV - 10kV were applied to the tissues and the impedance was measured over a frequency range. On the application of the electric field, a steep increase was observed at low frequencies; the membrane was very resistive and a low electric current traveled in the extracellular space surrounding the membrane [90]. At high frequencies, the resistance dropped, and the impedance approached zero, allowing the electric field to pass through the cell or tissue more uniformly. Also, the resistance was seen to decrease with the increasing number of pulses and applied voltage while the reactance increased. There was little to no difference between the impedance of tissues with a single pulse treatment and the no treatment group, signifying that a single pulse was not enough to cause substantial damage to the membrane. The potato tissues had an average percentage decrease of 44.4% after 80 pulses while the breast tumors had a decrease of 12.78% for 1000pulses and 22.27% for 1200pulses.

REFERENCES

1. Toepfl, S., Mathys, A., Heinz, V., & Knorr, D. Review: potential of high hydrostatic pressure and pulsed electric fields for energy efficient and environmentally friendly food processing. *Food Rev. Int*. **22,** 405–423. doi: 10.1080/87559120600865164 (2006b).
2. Raso, J. et al. Recommendations guidelines on the key information to be reported in studies of application of PEF technology in food and biotechnological processes. *Innov. Food Sci. Emerg. Technol*. **37,** 312–321. doi: 10.1016/j.ifset.2016.08.003 (2016).
3. Buchman, L. & Mathys, A. Perspective on Pulsed Electric Field Treatment in the Bio-based Industry. *Front. Bioeng. Biotechnol.* **7,** 265. Dio: 10.3389/fbioe.2019.00265 (2019).
4. Beebe, S. J. and Schoenbach, K. H. Nanosecond pulsed electric fields: A new stimulus to activate intracellular signaling. *J. Biomed. Biotechnol*. **4,** 297–300. doi: 10.1155/JBB.2005.297 (2005)
5. Hu Q. et. al. Simulations of transient membrane behavior in cells subjected to a high intensity ultrashort electric pulse. *Phys Rev E Stat Nonlin Soft Matter Phys*. **71,** (3 pt 1):031914. (2005)
6. Kotnik, T., Rems, L., Tarek, M. & Miklavcic, D. Membrane electroporation and electropermeabilization: mechanisms and models. *Annu. Rev. Biophys.* **48,** 63-91 (2019).
7. Wagstaff, P. G. et al. Irreversible electroporation: state of the art. *Onco Targets Ther*. **9,** 2437–2446. doi:10.2147/OTT.S88086 (2016).
8. Nollet, J. A. Recherches sur les causes particulieres des ph´enom´enes ´electriques. *Paris: Guerin & Delatour* (1754).
9. Ivorra, A. & Rubinsky, B. History review of irreversible electroporation in medicine. In: Rubinsky B, ed. Irreversible electroporation, series in biomedical engineering. Berlin: Chennai Springer-Verlag, 1–21 (2010).
10. Lee, R. C., Gaylor, D. C., Bhatt, D. & Israel, D. A. Role of cell membrane rupture in the pathogenesis of electrical trauma. J Surg Res. 44, 709–719 (1988).
11. Deipolyi, A, R. et al. Irreversible electroporation: evolution of a laboratory technique in interventional oncology. *Diagn Interv Radiol.* **20(2),** 147–154. doi:10.5152/dir.2013.13304 (2014).
12. Frankenhaeuser, B. & Wid´en, L. Anode break excitation in desheathed frog nerve. *J. Physiol.* **131,** 243–47 (1956).
13. Stampfli, R. & Willi, M. Membrane potential of a Ranvier node measured after electrical destruction of its membrane. *Experientia* **13,** 297–98 (1957).
14. Neumann, E., Schaefer-Ridder, M., Wang, Y. & Hofschneider, P. H. Gene transfer into mouse lyoma cells by electroporation in high electric fields. *EMBO J.* **1,** 841–45 (1982).
15. Gehl, J. Electroporation for medical use in drug and gene electrotransfer. In: Alkire RC, Dieter MK, Lipkowski J, eds. Advances in electrochemical science and engineering. Weinheim: Wiley-VCH Verlag GmgH & Co., 369–388 (2011)
16. Mir, L. M. et al. Electrochemotherapy, a new antitumor treatment: first clinical trial. *C. R. Acad. Sci. III* **313,** 613–18 (1991).
17. Okino, M. & Mohri, H. Effects of a high-voltage electrical impulse and an anticancer drug on in vivo growing tumors. *Jpn. J. Cancer Res. Gann.* **78,** 1319–21 (1987).

18. Orlowski, S., Belehradek, J. Jr., Paoletti, C. & Mir, L. M. Transient electropermeabilization of cells in culture: increase of the cytotoxicity of anticancer drugs. *Biochem. Pharmacol.* **37,** 4727–33 (1988).
19. Golberg, A. & Yarmush, M. L. Nonthermal irreversible electroporation: fundamentals, applications, and challenges. *IEEE Trans. Biomed. Eng.* **60,** 707–14 (2013).
20. Michael, D. H. & O'Neill, M, E. Electrohydrodynamic instability in plane layers of fluid. *J. Fluid Mech.* **41,** 571–80 (1970).
21. Cruzeiro-Hansson, L. & Mouritsen, O. G. Passive ion permeability of lipid membranes modelled via lipid-domain interfacial area. *Biochim. Biophys. Acta* **944,** 63–72 (1988).
22. Tsong, T. Y. Electroporation of cell membranes. *Biophys. J.* **60,** 297–306 (1991).
23. Tarek, M. Membrane electroporation: a molecular dynamics simulation. *Biophys. J.* **88,** 4045–53 (2005).
24. Kotnik, T. & Miklavˇciˇc, D. Theoretical evaluation of voltage inducement on internal membranes of biological cells exposed to electric fields. *Biophys. J.* **90,** 480–91 (2006).
25. Kotnik, T., Miklavˇciˇc, D. & Slivnik, T. Time course of transmembrane voltage induced by time-varying electric fields—a method for theoretical analysis and its application. *Bioelectrochem. Bioenerg.* **45,** 3–16 (1998).
26. Yarmush, M. L. et al. Electroporation-based technologies for medicine: principles, applications, and challenges. *Annual Review of Biomedical Engineering*. **16,** 295-320. 10.1146/annurev-bioeng-071813-104622 (2014).
27. Gumbart, J., Khalili-Araghi, F., Sotomayor, M. & Roux, B. Constant electric field simulations of the membrane potential illustrated with simple systems. *Biochim. Biophys. Acta* **1818,** 294–302 (2012).
28. Delemotte, L. & Tarek, M. 2012. Molecular dynamics simulations of lipid membrane electroporation. *J. Membrane Biol.* **245,** 531–43 (2012).
29. Kirsch, S. A. & Bockmann, R. A. Membrane pore formation in atomistic and coarse-grained simulations. *Biochim. Biophys. Acta* **1858,** 2266–77 (2016).
30. Weaver, J. C. & Chizmadzhev, Y. A. Theory of electroporation: a review. Bioelectrochem Bioenerg 42, 135–160 (1996).
31. Molotkovsky, R. J. & Akimov, S. A. Calculation of line tension in various models of lipid bilayer pore. *Biol. Membrany.* **26**, 149–158 (2009).
32. Akimov, S.A. *et al.* Pore formation in lipid membrane II: Energy landscape under external stress. *Sci Rep* **7,** 12509 (2017).
33. Levine, Z. A. & Vernier, P. T. Life cycle of an electropore: field-dependent and field-independent steps in pore creation and annihilation. *J. Membrane Biol.* **236,** 27–36 (2010).
34. Kotnik, T., Bobanovi´c, F. & Miklavˇciˇc, D. Sensitivity of transmembrane voltage induced by applied electric fields—a theoretical analysis. *Bioelectrochem. Bioenerg.* **43,** 285–91 (1997).
35. Teissie, J., Golzio, M. & Rols, M. P. Mechanisms of cell membrane electropermeabilization: a minireview of our present lack of knowledge. *Biochim. Biophys. Acta Gen. Subj.* **1724,** 270–280 (2005). doi: 10.1016/j.bbagen.2005.05.006
36. Aycock, K. N. & Davalos, K. N. Irreversible Electroporation: Background, Theory, and Review of Recent Developments in Clinical Oncology. *Bioelectricity.* 214-234 (2019).
37. Loew, L. M. Voltage sensitive dyes: measurement of membrane potentials induced by DC and AC electric fields. *Bioelectromagnetics.* **13,** 179–89 (1992).

38. Garcia, P. A., Rossmeisl, J. H. & Davalos, R. V. Electrical conductivity changes during irreversible electroporation treatment of brain cancer. Annual International Conference of the IEEE Engineering in Medicine and Biology Society (IEEE) 739–42
39. Wagstaff, P. G. et al. The efficacy and safety of irreversible electroporation for the ablation of renal masses: a prospective, human, in-vivo study protocol. *BMC Cancer*. **15,** 165 (2015)
40. Bertacchini, C. et al. Design of an irreversible electroporation system for clinical use. *Technol Cancer Res Treat*. **6,** 313–320 (2007).
41. Davalos, R. V., Mir, I. L. & Rubinsky, B. Tissue ablation with irreversible electroporation. Ann Biomed Eng. 33, 223–231 (2005).
42. Rosazza, C. et al. Gene Electrotransfer: A Mechanistic Perspective. *Curr Gene Ther*. **16(2),** 98–129 (2016). doi:10.2174/1566523216666160331130040
43. Cemazar, M. et al. Electrochemotherapy in veterinary oncology. *J. Vet. Intern. Med.* **22,** 826–31 (2008).
44. Miklavˇciˇc, D. et al. Electrochemotherapy: technological advancements for efficient electroporation-based treatment of internal tumors. *Med. Biol. Eng. Comput.* **50,** 1213–25 (2012).
45. Mir, L. M., Orlowski, S., Belehradek, J. Jr. & Paoletti, C. Electrochemotherapy potentiation of antitumour effect of bleomycin by local electric pulses. *Eur. J. Cancer* **27,** 68–72 (1991).
46. Heller, R. Treatment of cutaneous nodules using electrochemotherapy. *J. Fla. Med. Assoc.* **82,** 147– 50 (1995).
47. Sersˇa, G. et al. Electrochemotherapy with cisplatin: clinical experience in malignant melanoma patients. *Clin. Cancer Res.* **6,** 863–67 (2000).
48. Sersˇa, G., Cˇ emazˇar, M. & Miklavcˇicˇ, D. Antitumor effectiveness of electrochemotherapy with cisdiamminedichloroplatinum(II) in mice. *Cancer Res.* **55,** 3450–55 (1995).
49. Jaroszeski, M. et al. Toxicity of anticancer agents mediated by electroporation in vitro. *Anticancer Drugs.* **11(3),** 201-208 (2000).
50. Edhemovi´c, I. et al. Electrochemotherapy: a new technological approach in treatment of metastases in the liver. *Technol. Cancer Res. Treat.* **10,** 475–85 (2011).
51. Roux, S. et al. Tumor destruction using electrochemotherapy followed by CpG oligodeoxynucleotide injection induces distant tumor responses. *Cancer Immunol. Immunother.* **57,** 1291–300 (2008).
52. Gehl, J. Electroporation: theory and methods, perspectives for drug delivery, gene therapy and research. *Acta Physiol. Scand.* **177,** 437–47 (2003).
53. Mali, B. et al. Antitumor effectiveness of electrochemotherapy: a systematic review and meta-analysis. *Eur. J. Surg. Oncol.* **39,** 4–16 (2013).
54. Faurie, C. *et al.* Electro-mediated gene transfer and expression are controlled by the life-time of DNA/ membrane complex formation. *J Gene Med*. **12(1),** 117-25 (2010).
55. Golzio, M., Teissie, J. & Rols, M. P. Cell synchronization effect on mammalian cell permeabilization and gene delivery by electric field. *Biochim Biophys Acta* **1563(1-2)** 23-8 (2002).
56. Heller, L. C & Heller, R. In vivo electroporation for gene therapy. *Hum. Gene Ther.* **17,** 890–97 (2006).

57. Favard, C., Dean, D. S. & Rols, M. P. Electrotransfer as a non viral method of gene delivery. *Curr. Gene Ther.* **7,** 67–77 (2007).
58. Titomirov, A. V., Sukharev, S. & Kistanova, E. In vivo electroporation and stable transformation of skin cells of newborn mice by plasmid DNA. *Biochim. Biophys. Acta* **1088,** 131–34 (1991).
59. Heller, R. et al. In vivo gene electroinjection and expression in rat liver. *FEBS Lett.* **389,** 225–28 (1996).
60. Rols, M. P. et al. In vivo electrically mediated protein and gene transfer in murine melanoma. *Nat. Biotechnol.* **16,** 168–71 (1998).
61. Martel-Renoir, D. et al. Coelectrotransfer to skeletal muscle of three plasmids coding for antiangiogenic factors and regulatory factors of the tetracycline-inducible system: tightly regulated expression, inhibition of transplanted tumor growth and antimetastatic effect. *Mol. Ther.* **8,** 425–33 (2003).
62. Cichon, T. et al. Electrotransfer of gene encoding endostatin into normal and neoplastic mouse tissues: inhibition of primary tumor growth and metastatic spread. *Cancer Gene Ther.* **9,** 771–77 (2002).
63. Daud, A. I. et al. Phase I trial of interleukin-12 plasmid electroporation in patients with metastatic melanoma. *J. Clin. Oncol.* **26,** 5896–903 (2008).
64. Spanggaard, I. et al. Gene electrotransfer of plasmid antiangiogenic metargidin peptide (AMEP) in disseminated melanoma: safety and efficacy results of a Phase I first-in-man study. *Hum. Gene Ther. Clin. Dev.* **24(3),** 99–107 (2013).
65. Denet, A. R., Vanbever, R & Pr´eat, V. Skin electroporation for transdermal and topical delivery. *Adv. Drug Deliv. Rev.* **56,** 659–74 (2004).
66. Demiryurek, Y. et al. Transport, resealing, and re-poration dynamics of two-pulse electroporation-mediated molecular delivery. *Biochim. Biophys. Acta Biomembr.* **1848,** 1706–1714. (2015).
67. Davalos, R. V., Bhonsle, S. & Neal, R. E. 2nd. Implications and considerations of thermal effects when applying irreversible electroporation tissue ablation therapy. *Prostate*. **75(10),** 1114–1118 (2015). doi:10.1002/pros.22986
68. Maor, E., Ivorra, A., Leor, J & Rubinsky, B. The effect of irreversible electroporation on blood vessels. *Technol. Cancer Res. Treat.* **6,** 307–12 (2007).
69. Phillips, M. A., Narayan, R., Padath,T & Rubinsky, B. Irreversible electroporation on the small intestine. *Br. J. Cancer* **106,** 490–95 (2012).
70. Miller, L., Leor, J & Rubinsky, B. Cancer cells ablation with irreversible electroporation. *Technol. Cancer Res. Treat.* **4,** 699–705 (2005).
71. Edd, J. F. In vivo results of a new focal tissue ablation technique: irreversible electroporation. *IEEE Trans. Biomed. Eng.* **53,** 1409–15 (2006).
72. Rubinsky, B., Onik, G. & Mikus, P. Irreversible electroporation: a new ablation modality—clinical implications. *Technol. Cancer Res. Treat.* **6,** 37–48 (2007).
73. Martin, R. C. G., McFarland, K., Ellis, S. & Velanovich, V. Irreversible electroporation therapy in the management of locally advanced pancreatic adenocarcinoma. *J. Am. Coll. Surg.* **215,** 361–69 (2012).
74. Neal, R. E. II et al. In vitro and numerical support for combinatorial irreversible electroporation and electrochemotherapy glioma treatment. *Ann Biomed Eng.* **42(3),** 475–487 (2014).

75. Lee, E. W., Loh, C. T. & Kee, S. T. Imaging guided percutaneous irreversible electroporation: Ultrasound and immunohistological correlation. *Technol Cancer Res Treat* **6(4),** 287–294 (2007).
76. Neal, R.E. II. et al. Improved local and systemic anti-tumor efficacy for irreversible electroporation in immunocompetent versus immunodeficient mice. PLoS ONE **8(5),** e64559 (2013).
77. Garcia, P. A., Davalos, R. V. & Miklavcic, D. A numerical investigation of the electric and thermal cell kill distributions in electroporation-based therapies in tissue. PLoS ONE **9(8),** e103083 (2014).
78. Wang, R. Y. et al. Study on fish embryo responses to the treatment of cryoprotective chemicals using impedance spectroscopy. *Eur Biophys J.* (2005).
79. Suselbeck, T. et al. Intravascular electric impedance spectroscopy of atherosclerotic lesions using a new impedance catheter system. *Basic Res Cardil* **100,** 446–452 (2005)
80. Soley, A. et al. On-line monitoring of yeast cell growth by impedance spectroscopy. *Jl of Biotechnology* **118,** 398–405 (2005).
81. Halter, R. et al. Electrical Impedance Spectroscopy of the Human prostate. *IEEE Trans Biomedical Engineering* **54(7),** (2007).
82. Kerner, T. E. et al. Electrical impedance spectroscopy of the breast: clinical imaging results in 26 subjects. *IEEE Trans Medical Imaging.* **21(6),** 638–45 (2002).
83. Golberg, A., Laufer, S., Rabinowitch, H. D. & Rubinsky, B. In vivo non-thermal irreversible electroporation impact on rat liver galvanic apparent internal resistance. *Phys. Med. Biol.* **56,** 951–63 (2011).
84. Kranjc, M. et al. Ex vivo and in silico feasibility study of monitoring electric field distribution in tissue during electroporation based treatments. *PLoS ONE* **7,** e45737 (2012).
85. Ivorra, A., Mir, L. M. & Rubinsky, B. Electric field redistribution due to conductivity changes during tissue electroporation: experiments with a simple vegetal model. In: *World Congress on medical physics and biomedical engineering*. 59–62 (2009).
86. Dean, D.A., Ramanathan, T., Machado, D. & Sundararajan, R. Electrical Impedance Spectroscopy Study of Biological Tissues. *J Electrostat.* **66(3-4),** 165–177 (2008). doi:10.1016/j.elstat.2007.11.005
87. Ivorra, A. et al. Minimally invasive silicon probe for electrical impedance measurements in small animals. *Biosensors and Bioelectronics* **391,** 391-39 (2003).
88. IEC. Expression of performance of electrochemical analyzers, Part 3: Electrolytic conductivity. IEC Publication 607046 (2002).
89. Gersing, E. Impedance spectroscopy on living tissue for determination of the state of organs. *Bioelectrochemsitry and Bioenergetics.* **45,** 145–149 (1998).
90. Cole, K. S. Electric phase angle of cell membranes. *J Gen Physiol.* **15,** 641-649 (1932). doi:10.1085/jgp.15.6.641
91. Pavlin, M. et al. Effect of cell electroporation on the conductivity of a cell suspension. *Biophys J*. **88(6),** 4378–4390 (2005) doi:10.1529/biophysj.104.048975

APPENDIX

STATISTICAL ANALYSIS

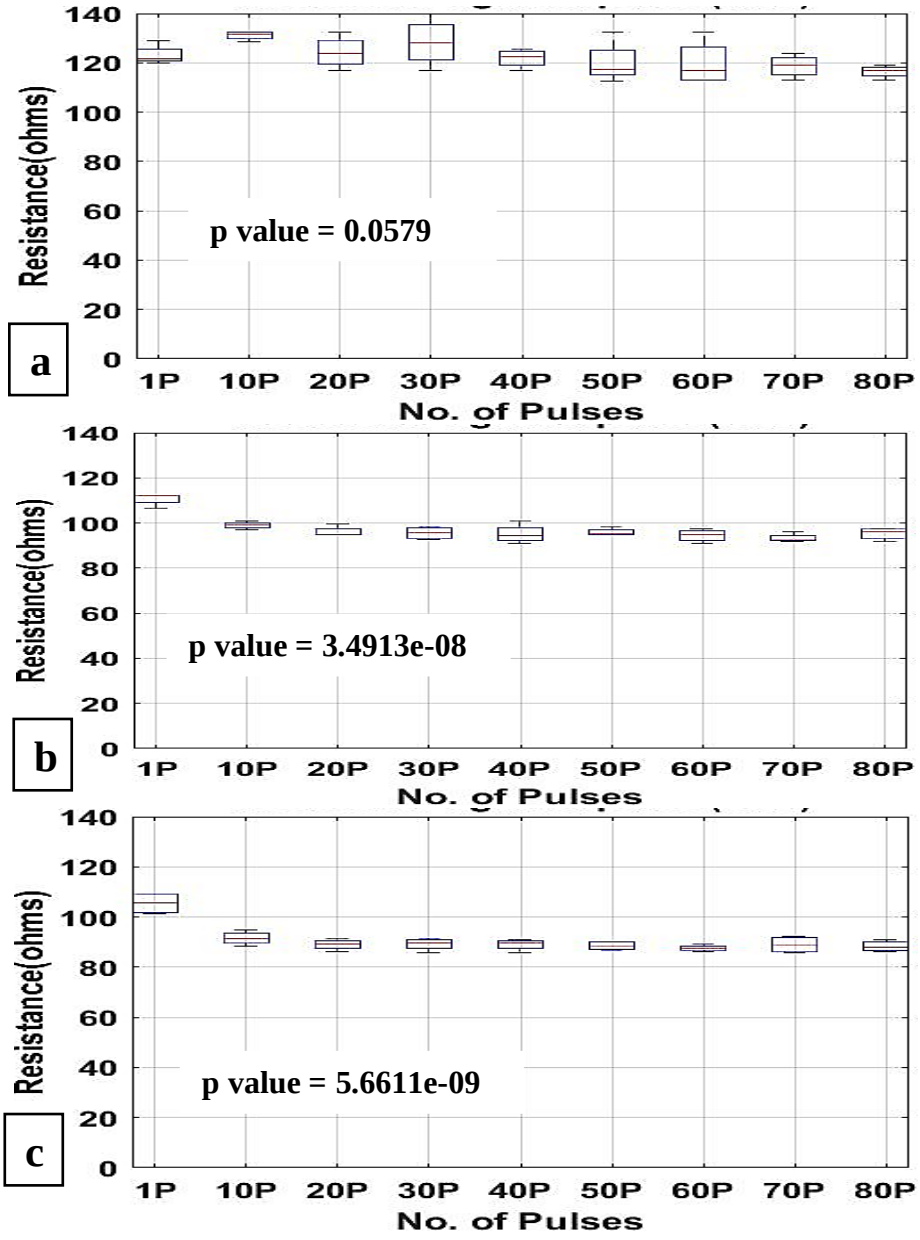

Figure 16: Resistance Trend Obtained from V-I Monitor. (a) at 1kV, a wide range of variation is observed, showing no significant drop in resistance. (b) 3kV and (c) 5kV shows less variation. The p values for 1kV, 3kV, and 5kV are 0.0579, 3.4913e-08, and 5.6611e-09 respectively.

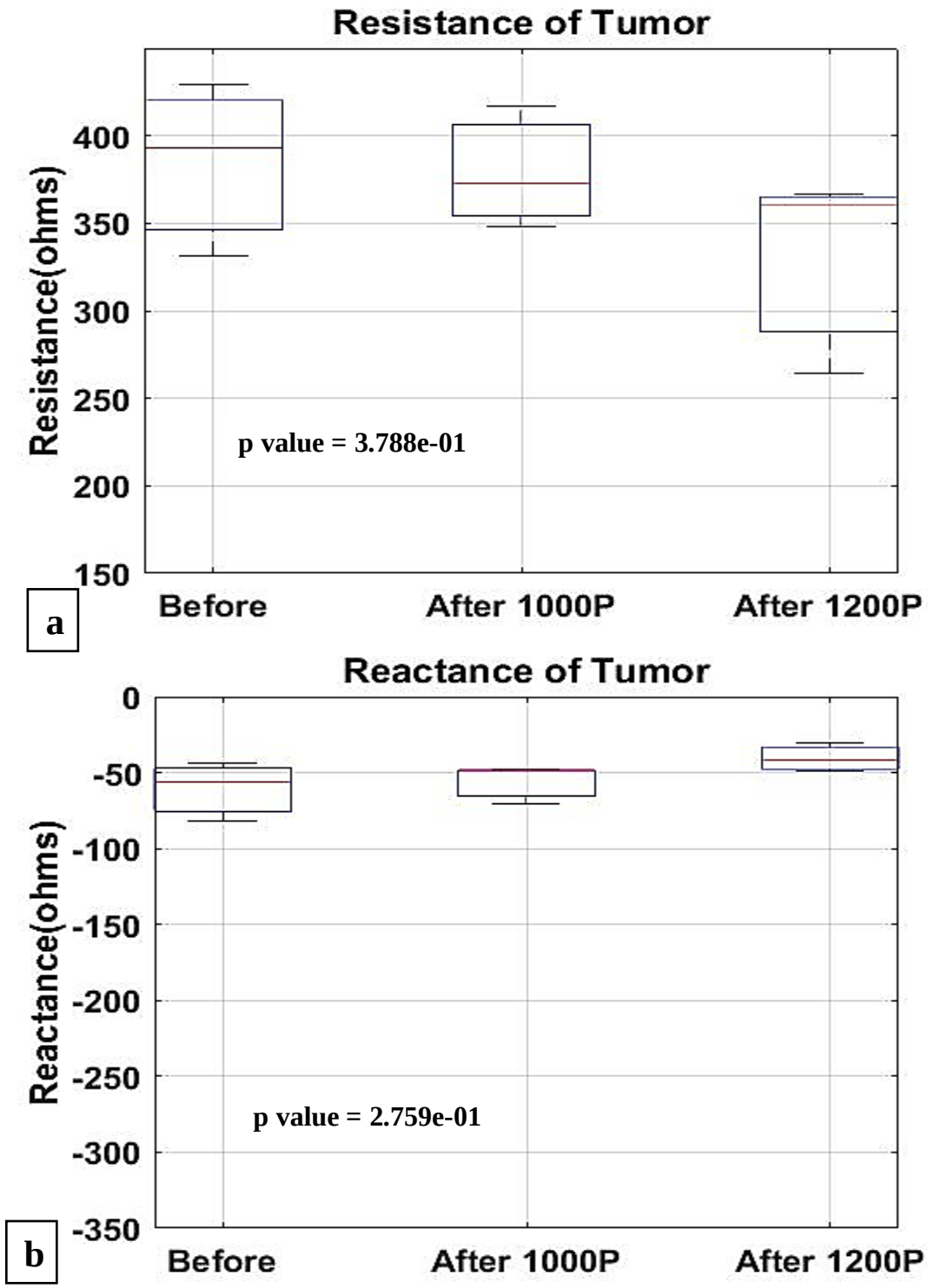

Figure 17: Variation in the Resistance and Reactance of Tumor Tissue Measured Before, After 1000pulses and After 1200 Pulses.

VITA

Edwin Ayobami Oshin
Department of Biomedical Engineering
Old Dominion University
Norfolk, VA 23529

EDUCATION

Bachelor of Engineering Electrical & Electronics Engineering
Afe Babalola University
Ekiti, Nigeria
October 2018

EXPERIENCE

Edwin Oshin has worked in an electrical maintenance and repair company, gaining experience in how electrical appliances function. He also worked in a plastic furniture making company and gained experience working as a research assistant at Frank Reidy Research Center for Bioelectrics, Old Dominion University.